

Nuclear Criticality Safety of the DOT 9975 Container for $^{237}\text{NpO}_2$ Storage, Handling, and Transport

August 2003

Prepared by

**D. A. Reed
S. Goluoglu
C. M. Hopper
R. M. Wham**

DOCUMENT AVAILABILITY

Reports produced after January 1, 1996, are generally available free via the U.S. Department of Energy (DOE) Information Bridge:

Web site: <http://www.osti.gov/bridge>

Reports produced before January 1, 1996, may be purchased by members of the public from the following source:

National Technical Information Service
5285 Port Royal Road
Springfield, VA 22161
Telephone: 703-605-6000 (1-800-553-6847)
TDD: 703-487-4639
Fax: 703-605-6900
E-mail: info@ntis.fedworld.gov
Web site: <http://www.ntis.gov/support/ordernowabout.htm>

Reports are available to DOE employees, DOE contractors, Energy Technology Data Exchange (ETDE) representatives, and International Nuclear Information System (INIS) representatives from the following source:

Office of Scientific and Technical Information
P.O. Box 62
Oak Ridge, TN 37831
Telephone: 865-576-8401
Fax: 865-576-5728
E-mail: reports@adonis.osti.gov
Web site: <http://www.osti.gov/contact.html>

This report was prepared as an account of work sponsored by an agency of the United States Government. Neither the United States government nor any agency thereof, nor any of their employees, makes any warranty, express or implied, or assumes any legal liability or responsibility for the accuracy, completeness, or usefulness of any information, apparatus, product, or process disclosed, or represents that its use would not infringe privately owned rights. Reference herein to any specific commercial product, process, or service by trade name, trademark, manufacturer, or otherwise, does not necessarily constitute or imply its endorsement, recommendation, or favoring by the United States Government or any agency thereof. The views and opinions of authors expressed herein do not necessarily state or reflect those of the United States Government or any agency thereof.

**NUCLEAR CRITICALITY SAFETY OF THE DOT 9975 CONTAINER
FOR ²³⁷NpO₂ STORAGE, HANDLING, AND TRANSPORT**

Author(s)

**D. A. Reed
S. Goluoglu
C. M. Hopper
R. M. Wham**

Date Published: August 2003

Prepared by
OAK RIDGE NATIONAL LABORATORY
P.O. Box 2008
Oak Ridge, Tennessee 37831-6285
managed by
UT-Battelle, LLC
for the
U.S. DEPARTMENT OF ENERGY
under contract DE-AC05-00OR22725

CONTENTS

	Page
LIST OF FIGURES	v
LIST OF TABLES	vii
ACRONYMS	ix
ACKNOWLEDGEMENTS	xi
EXECUTIVE SUMMARY.....	xiii
1. OBJECTIVE	1
2. METHODOLOGY	2
3. THE CRITICALITY PHYSICS OF ²³⁷ Np	3
3.1 INTRODUCTION	3
3.2 NUCLEAR DATA FOR ²³⁷ Np	3
3.3 THE EFFECT OF NEUTRON MODERATORS	7
3.4 ANSI/ANS-8.15 COMPUTED DATA AND CURRENT RESULTS	8
3.5 THE EFFECT OF OXIDE DENSITIES LESS THAN THEORETICAL	9
4. DOT 9975 CONTAINER DESCRIPTION	14
5. THE CRITICALITY SAFETY OF AN INDIVIDUAL ²³⁷ NP CONTAINER	17
6. CRITICALITY SAFETY OF ARRAYS OF ²³⁷ NP CONTAINERS	18
6.1 NCS BASED ON MODERATION BY INSULATION MATERIALS	18
6.2 NCS BASED ON LIMITED EFFECTIVE DENSITY OF THE ²³⁷ NpO ₂	20
6.3 NCS BASED ON LIMITED MASS (INDIVIDUAL TRANSPORT OPERATIONS)	21
6.4 NCS OF MATERIAL RELEASES	21
7. CRITICALITY SAFETY OF COMMINGLED STORAGE OF ²³⁷ NP CONTAINERS AND CONTAINERS OF HIGHLY ENRICHED URANIUM	22
7.1 EXPECTED EFFECT OF DOT 9975 CONTAINERS ON HEU STORAGE	22
7.2 COMPUTATIONAL CHECK FOR INTERACTION OF DOT 9975 CONTAINERS AND HEU	22
8. ABNORMAL CONDITIONS AND EVENTS THAT ARE BOUNDED BY THE CRITICALITY SAFETY CONSIDERATIONS	24
9. CONCLUSION	25
REFERENCES	27

CONTENTS (continued)

APPENDIX A. SCOPING COMPUTATIONS FOR k_{∞} FOR ^{237}Np -H₂O MIXTURES.....A1

APPENDIX B. SCOPING COMPUTATIONS BASED ON ANSI/ANS-8.15 DATA.....B1

APPENDIX C. SCOPING COMPUTATIONS FOR DOT 9975 SINGLE UNITS AND
INFINITE ARRAYSC1

APPENDIX D. COMPUTATIONS OF CRITICAL EXPERIMENTS INVOLVING
HEU METAL CYLINDERS IN ARRAYS.....D1

APPENDIX E. SCOPING COMPUTATIONS FOR ADJACENT ARRAYS OF DOT 9975
CONTAINERS AND HEU UNITS.....E1

LIST OF FIGURES

Figure		Page
1	Energy-Dependent Neutron Cross Section Data for ^{237}Np (Continuous Energy)	4
2	Energy-Dependent Neutron Cross Section Data for ^{237}Np (Energy Group Format).....	5
3	Density Exponents of Unmoderated Spherical Cores in Constant-Density Reflectors.....	10
4	Calculated Core-Density Exponents for Water-Moderated Spheres of Homogeneous Metal-Water Mixtures	11
5	The 9975 Package Details (cross sectional view of vertical cylinder).....	15
6	NCS Model for the DOT 9975 Container with 6 kg ^{237}Np as Oxide at Half Theoretical Density.....	16

LIST OF TABLES

Table		Page
1	Nuclear Data of Criticality Interest for ^{237}Np	6
2	Computed Infinite-System Neutron Multiplication Factors (k_{∞}) for ^{237}Np -H ₂ O Homogeneous Mixtures (Scale 4.4a Results).....	7
3	Computed Critical Mass Estimates for ^{237}Np in Spherical Geometry (SCALE 4.4a)	8
4	Comparison of Reflector Effects for ^{235}U as Highly Enriched Uranium Metal and for $^{237}\text{NpO}_2$, Material in Spherical Geometry at Theoretical Density	11
5	Current Work: Computed Core Density Exponents for $^{237}\text{NpO}_2$	12

ACRONYMS

BWXT Y-12, L.L.C.	BWXT Y-12 Limited Liability Company
CFR	Code of Federal Regulations
COC	Certificate of Compliance
DOE	Department of Energy
DOT	Department of Transportation
DSA	documented safety analysis
FAB	Facility Authorization Basis
HEU	highly enriched uranium (generally > 90% ²³⁵ U)
NCS	nuclear criticality safety
ORNL	Oak Ridge National Laboratory
ORR	Oak Ridge Reservation
PCV	Primary Containment Vessel
REDC	Radiochemical Engineering Development Center
RHU	radioisotope heater unit
SAR	Safety Analysis Report
SARP	Safety Analysis Report for Packaging
SCV	Secondary Containment Vessel
SRS	Savannah River Site
Y-12 NSC	Y-12 National Security Complex
WSRC	Westinghouse Savannah River Company

ACKNOWLEDGEMENTS

The authors wish to express appreciation to D. E. Mueller, R. G. Taylor, and R. M. Westfall for technical and editorial review, and to S. L. Lay for assistance in final preparation of the report for publication.

EXECUTIVE SUMMARY

Nuclear criticality safety considerations are presented to address use of the DOT 9975 shipping container for $^{237}\text{NpO}_2$.

The DOT 9975 container will be used by multiple DOE sites and contractors. Various of site- and activity-specific NCS and facility safety documents are yet to be developed. For these reasons, an overall assessment of criticality safety of $^{237}\text{NpO}_2$ -loaded DOT 9975 containers is considered useful to personnel involved in generating, reviewing, or approving these various documents.

It is concluded that inherent container features, the loading per container (maximum of 6 kg ^{237}Np), and the nuclear physics properties of $^{237}\text{NpO}_2$ combine to preclude the potential for a nuclear criticality accident. This conclusion applies to storage, handling, and transport operations involving closed DOT 9975 packages, including credible off-normal conditions that may result in damage to packages during those operations.

1. OBJECTIVE

The objective of this report is to demonstrate that the DOT 9975 shipping container may be used for storage, handling, and transport of $^{237}\text{NpO}_2$ without potential for a nuclear criticality accident.

Prior to shipment of the material from the Department of Energy (DOE) Savannah River Site (SRS) to the Y-12 National Security Complex (Y-12 NSC), a Safety Analysis Report for Packaging (SARP) will be prepared to address specific nuclear criticality safety (NCS) criteria identified in the United States Code of Federal Regulations (CFR), 10 CFR 71. The SARP effort must include derivation of a "criticality index" to be assigned to each package for purposes of NCS during public highway transport.

The Y-12 NSC (currently managed by the BWXT-Y-12, L.L.C) will provide secure storage for the DOT 9975 packages until the material is needed by Oak Ridge National Laboratory (ORNL). In preparation for that effort, internal Y-12 NSC NCS approval or evaluation documents must be generated; internal Y-12 NSC facility safety documentation (such as Safety Analysis Reports, SARs) must be revised or developed.

A large fraction of the DOT 9975 containers may remain in storage for many years at the Y-12 NSC. It is likely that the Department of Transportation Certificate of Compliance (DOT COC) for $^{237}\text{NpO}_2$ loadings in the DOT 9975 will not be formally maintained (renewed). If so, subsequent transports of DOT 9975 packages to ORNL would be conducted as an on-site transport activity. As described by 10 CFR 830 Subpart B, such an activity would require a documented safety analysis (DSA) in the form of a DOE-approved on-site transportation plan. The DSA would be supported by NCS documentation.

Once ORNL commences production operations for ^{238}Pu , some inventory of loaded DOT 9975 containers will be handled or stored at ORNL facilities. Internal ORNL NCS approval or evaluation documents and ORNL facility safety documentation are yet to be generated for these activities.

Thus, multiple DOE sites and contractors will use the DOT 9975 container for $^{237}\text{NpO}_2$. A variety of site- and activity-specific NCS and facility safety documents are yet to be developed. For these reasons, an overall assessment of criticality safety of $^{237}\text{NpO}_2$ -loaded DOT 9975 containers is considered useful to personnel involved in generating, reviewing, or approving the various NCS and facility safety documents.

This report serves to demonstrate to project management, to technical staff, and to regulatory oversight personnel that the DOT 9975 container may be employed for $^{237}\text{NpO}_2$ storage, handling, and transport operations without potential for a nuclear criticality accident.

2. METHODOLOGY

The primary NCS methodologies of this assessment are (1) consideration of the nuclear physics of ^{237}Np under moderated conditions, and (2) application of the single-unit steel-reflected subcritical limit value for $^{237}\text{NpO}_2$ provided by ANSI/ANS-8.15¹, *American National Standard Nuclear Criticality Control of Special Actinide Elements*. For some conditions, the ANSI/ANS-8.15 subcritical limit is adjusted using the "core-density" technique as described in standard NCS references.

NCS computations are utilized to provide confirmation and insight for these primary methods of assessment. However, the computations are not used to determine subcritical limits. No currently calculated effective neutron multiplication factor (k_{eff}) is employed as the sole basis for any NCS conclusion of this assessment. Thus, NCS code validation requirements of ANSI/ANS-8.1², *American National Standard Nuclear Criticality Safety in Operations with Fissionable Materials Outside Reactors*, are not applicable.*

Critical experiment data may be considered essential to meeting the NCS code validation requirements of ANSI/ANS-8.1. To-date, no critical experiments involving ^{237}Np as the primary fissionable material have been performed[†]. The primary purpose of ANSI/ANS-8.15 is to provide peer-reviewed, consensus subcritical limits for special actinides for which critical experiment data is not available. To compensate for unavailability of such data, the limits of ANSI/ANS-8.15 are derived in a manner to assure significant conservatism.

For consideration of large arrays of DOT 9975 containers loaded with $^{237}\text{NpO}_2$, the two primary NCS methodologies serve to *independently* confirm subcriticality of the arrays, based on two distinct and unrelated array characteristics. These characteristics are the inherent presence of neutron moderator materials within the containers, and the low overall $^{237}\text{NpO}_2$ density (as averaged over the array volumes). There is no feasible mechanism where either array characteristic may be sufficiently compromised to invalidate the individual conclusion of each method.

The application of dual NCS arguments based on independent array characteristics provides rigorous assurance of subcriticality for $^{237}\text{NpO}_2$ -loaded DOT 9975 container arrays.

* Although currently reported NCS computations may not be considered "validated" according to ANSI/ANS-8.1, the computational methods do represent contemporary techniques. The two codes employed are the MCNP code (Monte Carlo N-Particle Code, Version 4c2³) and the KENO-V.a code (CSAS4 and CSAS25 routines) of the SCALE Code System, Version 4.4a⁴. The neutron cross section libraries used for each code are primarily based on ENDF/B-V data (Evaluated Nuclear Data File/B-V). Both computational methods utilized ENDF/B-VI data for ^{16}O . Both codes are installed on a Digital AlphaStation DS10 with a EV67/600 617-MHz central processor unit. An initial verification of each code was performed upon installation of the software, and quarterly re-verification of each code is conducted for quality assurance purposes. The computer and software are maintained under the administrative control of the Nuclear Criticality Safety Group of the Operational Safety Services Division of ORNL.

[†] The lack of experimental data may be attributed to the large inventory of ^{237}Np required for such experiments, and the fact that historical activities involving ^{237}Np have not challenged conservative single-unit subcritical limits for ^{237}Np .

3. THE CRITICALITY PHYSICS OF ^{237}Np

3.1 INTRODUCTION

^{237}Np is a fissionable nuclide. Given an adequate inventory of materials containing ^{237}Np , with appropriate material forms and environmental conditions, nuclear criticality may be achieved.

This assessment focuses on the potential for an inadvertent, self-sustaining, neutron-induced fission chain reaction (criticality accident) involving DOT 9975 containers of $^{237}\text{NpO}_2$.*

ANSI/ANS-8.15[†] describes typical characteristics of actinide isotopes that contain an even number of neutrons[†]:

"Those [actinide isotopes] with an even number of neutrons ... can in many cases be made critical, but the mass required may be kilograms. The effect of moderation on these nuclides, such as in an aqueous solution, is to prevent - rather than enhance - criticality. These nuclides characteristically exhibit rather sharp thresholds in their fission cross sections, with little or no probability for subthreshold fission. As a consequence, the value of k_∞ will be reduced if even a small quantity of hydrogen is mixed uniformly with the element."

^{237}Np contains an even number of neutrons and exhibits a fission threshold, stated by ANSI/ANS-8.15 to be ~ 600 keV ($\sim 6 \times 10^5$ electron volts).

3.2 NUCLEAR DATA FOR ^{237}Np

Figure 1 graphically depicts the energy-dependent neutron cross section behavior of ^{237}Np , obtained from the Japanese Evaluated Nuclear Data Library (JENDL-3.2, 1997)[‡]. The units of the cross section data are in "barns," defined as 10^{-24} cm^2 .

Consider the fission cross section (σ_{fission} or σ_f). An appreciable ^{237}Np fission cross section (~ 1 barn or greater) continuously exists only above neutron energies of ~ 700 keV. It is notable that both the magnitude and the shape of σ_f for ^{237}Np , in the range of ~ 700 keV to 10 MeV, is *very* similar to that for ^{235}U . (A graphical depiction of the ^{235}U data is presented on Fig. 3-3 of Lamarsh's text, Nuclear Reactor Theory⁵.)

* A heavy metal content of Pu plus U of up to 1% of the neptunium weight is assumed to be negligible to NCS conclusions of this assessment. The $^{237}\text{NpO}_2$ is expected to contain very low levels of Pu and U (at ~ 0.5 weight % total), plus decay daughters of the Pu, U, and Np nuclides.

[†] Extracted from American National Standard ANSI/ANS-8.15-1981 (R1995) with permission of the publisher, the American Nuclear Society.

[‡] During this work, the JENDL-3.2 data was accessible via internet at the "T-2 Information Service" website of Los Alamos National Laboratory (<http://t2.lanl.gov/>)

As the neutron energy decreases one order of magnitude, from 1 MeV to 100 keV, the ^{237}Np fission cross section decreases nearly two orders of magnitude. In addition, as the neutron energy decreases, the ^{237}Np capture cross section (σ_{capture} or σ_{γ} , for transmutation to ^{238}Pu) rapidly increases. At 100 keV, σ_{γ} exceeds σ_f by an order of magnitude, and remains much greater than σ_f throughout lesser neutron energy ranges. [Since Fig. 1 presents considerable cross section detail in the resonance energy range (~ 0.05 eV to 100 eV), an energy-group-format presentation of the same cross section data is provided as Fig. 2.]

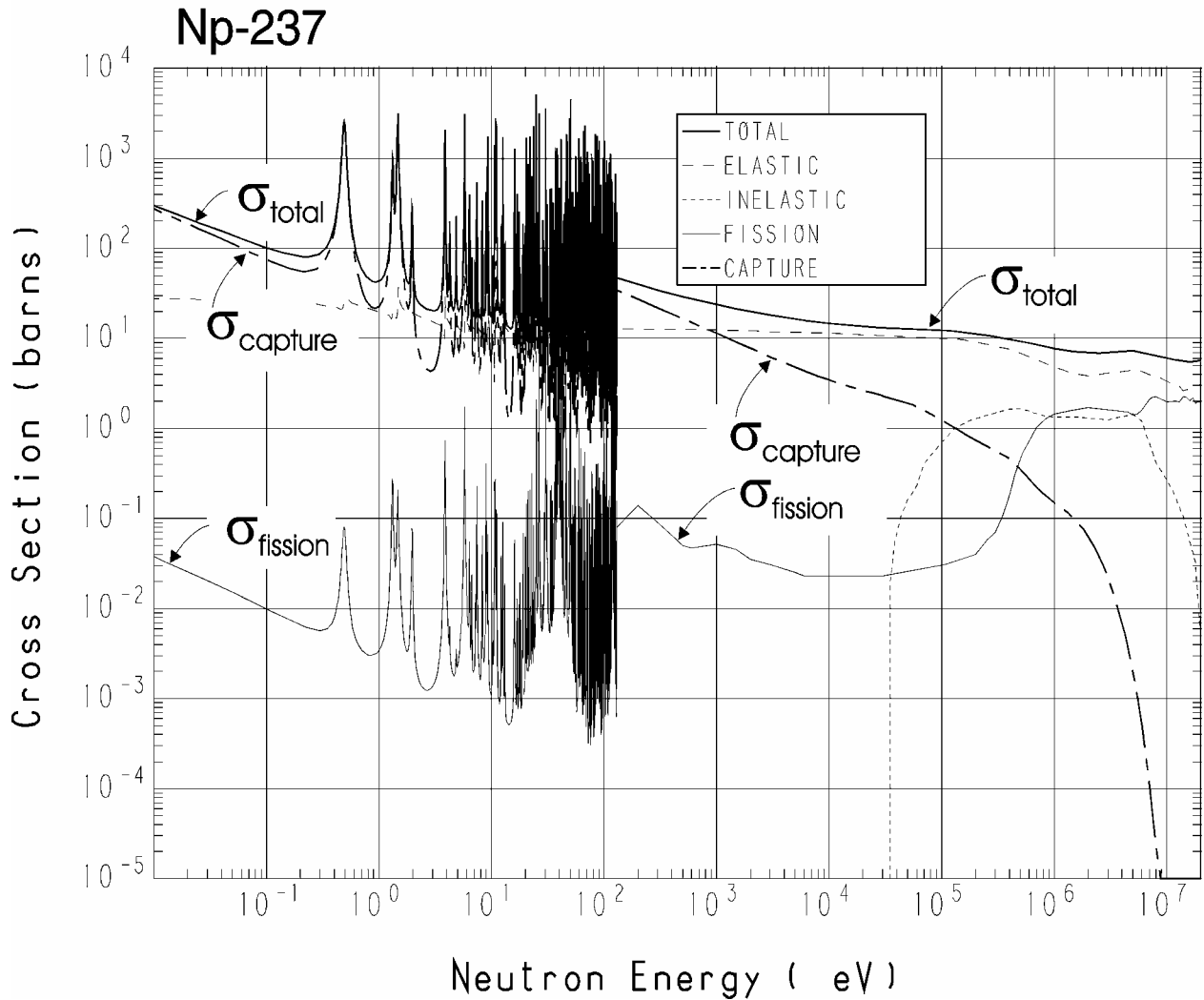


Fig. 1. Energy-Dependent Neutron Cross Section Data for ^{237}Np (Continuous Energy).

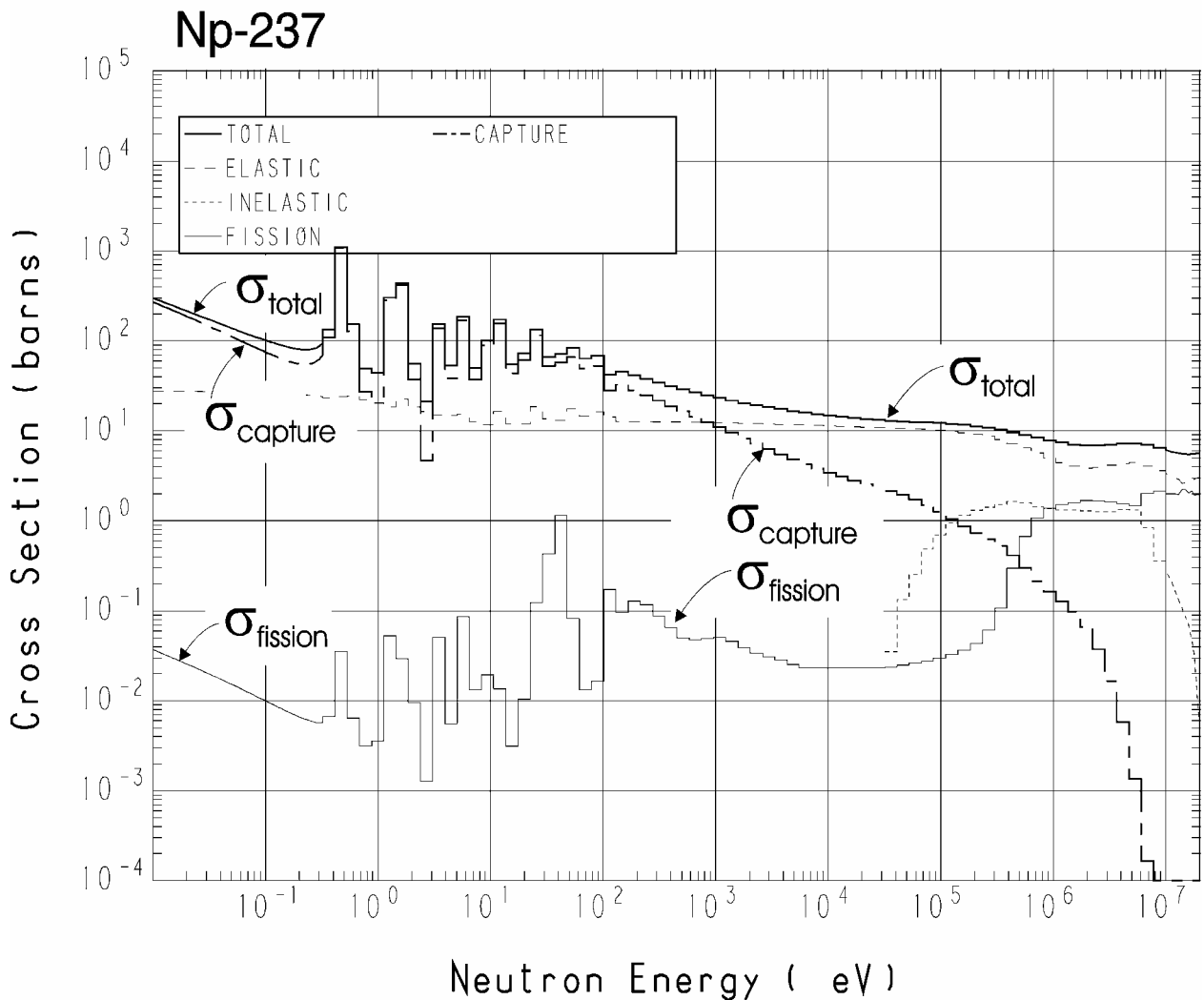


Fig. 2. Energy-Dependent Neutron Cross Section Data for ²³⁷Np (Energy Group Format).

Table 1 (below) depicts nuclear data of criticality interest for the 1 MeV to 100 keV neutron energy range, obtained from Release 8 of the ENDF/B-VI Library of Evaluated Nuclear Data File.* The numerical values of σ_f and σ_γ are as reported by the source. Tabulated data for ν (the average number of neutrons produced per fission, including both prompt and delayed neutrons) are provided only at a few discrete, widely separated energies by the source. In general, the value of ν for fissionable nuclides is a linear function of neutron energy over a very wide range of neutron energies. The source data for ²³⁷Np appears linear from thermal neutron energies up to 20 MeV. Thus, linear interpolation was employed to determine Table 1 values of ν .

* During this work, the ENDF/B-VI data was accessible via internet at the "T-2 Information Service" website of Los Alamos National Laboratory (<http://t2.lanl.gov/>).

Computed values of Table 1 (in bold text) include α ($= \sigma_\gamma / \sigma_f$) representing the "capture-to-fission ratio", and η ($= \nu / (1 + \alpha)$) representing the average number of fission neutrons produced per neutron absorption in ^{237}Np .

Table 1. Nuclear Data of Criticality Interest for ^{237}Np

Neutron Energy (MeV)	σ_f (barns)	σ_γ (barns)	ν (neutrons per ^{237}Np fission)	α (capture to fission ratio)	η (neutrons per ^{237}Np absorption)
4.0	1.555	0.022	3.235	0.014	3.190
3.0	1.639	0.033	3.085	0.020	3.025
2.0	1.676	0.061	2.936	0.036	2.833
1.0	1.456	0.173	2.786	0.119	2.490
0.9	1.322	0.193	2.771	0.146	2.418
0.8	1.232	0.216	2.756	0.175	2.345
0.7	1.017	0.255	2.741	0.251	2.191
0.6	0.747	0.315	2.726	0.422	1.917
0.5	0.447	0.414	2.711	0.927	1.407
0.4	0.183	0.548	2.696	2.996	0.675
0.3	0.070	0.681	2.681	9.729	0.250
0.2	0.0339	0.816	2.666	24.082	0.106
0.1	0.0161	1.210	2.651	75.180	0.035

The effective value of η for a fissionable nuclide must be at least unity in order for a critical chain reaction to be possible. In an assembly of fissionable material, η must somewhat exceed unity, sometimes by a substantial amount, to compensate for neutron loss mechanisms such as neutron leakage from the fissionable material configuration, or neutron absorption in non-fissionable materials that may be distributed among the fissionable material.

About 16% of the neutrons born in ^{237}Np fission have energies below the 600 keV threshold for ^{237}Np fission. The η values of Table 1 represent all neutrons born in fission, without regard as to whether those fission neutrons can perpetuate a neutron chain reaction. The "effective" values of η (for consideration of criticality potential) are thus $\sim 16\%$ less than the values shown on Table 1.

The Table 1 energy dependence of σ_f , σ_γ , and η for ^{237}Np is consistent with the ANSI/ANS-8.15 statement that the fission threshold for ^{237}Np is ~ 600 keV.

3.3 THE EFFECT OF NEUTRON MODERATORS

The ENDF/B-VI Library also provides the energy spectrum for neutrons from ^{237}Np fission. The spectrum is quite similar to that for ^{235}U . For ^{237}Np , the most probable energy for fission neutrons is about 750 to 900 keV, and the average energy is about 1.6 MeV. For ^{235}U , the most probable energy is about 730 keV and the average energy is about 2.0 MeV.

To illustrate the relationship between the fission threshold and presence of neutron moderators, consider the intermixing of small amounts of water with ^{237}Np . From Foster and Wright's text, Basic Nuclear Engineering,⁶ the average logarithmic energy decrement (ξ) for H_2O is 0.920. This value represents the average change in the logarithm of neutron energy per collision with a water molecule. The average number of collisions with water required to reduce a neutron from an energy of 1.6 MeV (average energy of a neutron born in ^{237}Np fission) to 600 keV (the ^{237}Np fission threshold) is given by n :

$$n = \frac{\ln(E_{\text{initial}} / E_{\text{final}})}{\xi} = \frac{\ln(1.6 / 0.6)}{0.920} = 1.1$$

This roughly indicates that for neutrons born by fission of ^{237}Np , an average of about one collision with a water molecule is adequate to decrease the neutron energy to the ^{237}Np fission threshold.

Scoping calculations described in Appendix A were used to obtain estimates of infinite-system neutron multiplication factors for idealized, homogeneous mixtures of ^{237}Np and H_2O or $^{237}\text{NpO}_2$ and H_2O . While there is inadequate critical experiment data to validate these results, the computed results are consistent with ANSI/ANS-8.15 prediction that uniform mixture of even a small quantity of hydrogen will reduce k_∞ of those actinides that exhibit fission thresholds.

The moderation ratios (H: ^{237}Np atom ratios) presented by Table 2 are significantly less than those that may result if $^{237}\text{NpO}_2$ powder is wetted by water. For instance, if $^{237}\text{NpO}_2$ oxide at 50% of theoretical density is water-immersed, intermixed water may exist at a volume fraction of 0.5. The resulting H: ^{237}Np atom ratio is 2.7. Table 2 indicates that $k_\infty < 1$ if the H: ^{237}Np atom ratio of neptunium materials is ~ 1 or greater.

Table 2. Computed Infinite-System Neutron Multiplication Factors (k_∞) for ^{237}Np - H_2O or $^{237}\text{NpO}_2$ - H_2O Homogeneous Mixtures (SCALE 4.4a Results)

H: ^{237}Np Atom Ratio	k_∞ for ^{237}Np - H_2O	k_∞ for $^{237}\text{NpO}_2$ - H_2O
0.0	1.62	1.34
0.5	1.15	1.02
1.0	0.92	0.84
1.5	0.78	0.71
2.0	0.67	0.62

Table 2 also indicates that presence of oxygen (e.g., due to the neptunium being in oxide form) reduces the criticality potential of ^{237}Np . Even though the value of ξ for oxygen is only 0.12, those neutrons born at energies slightly above the fission threshold may be rendered nonproductive (for future fissions) due to just one or two scattering collisions with oxygen.

3.4 ANSI/ANS-8.15 COMPUTED DATA AND CURRENT RESULTS

Appendix B of ANSI/ANS-8.15 provides computed estimates of critical masses for ^{237}Np metal and $^{237}\text{NpO}_2$ in single-unit, spherical geometry, unreflected and with stainless steel reflection. Appendix B of this report describes estimation of critical masses for those same conditions, performed using current computational methods. Table 3 summarizes the ANSI/ANS-8.15 estimates for comparison to current results obtained with SCALE 4.4a.

Table 3. Computed Critical Mass Estimates for ^{237}Np in Spherical Geometry (SCALE 4.4a)
(Summary of data provided in Appendix B, Section B.5)

Material Form	Reflector	ANSI/ANS-8.15 Data (kg ^{237}Np)	Current Results (kg ^{237}Np)
^{237}Np metal	None	56, 60, and 88	68.1 (within range of ANSI/ANS-8.15 values)
^{237}Np metal	SS304L	33, 38, and 55	40.8 (within range of ANSI/ANS-8.15 values)
$^{237}\text{NpO}_2$	None	288	337 (16% greater than ANSI/ANS-8.15 value)
$^{237}\text{NpO}_2$	SS304L	187	216 (16% greater than ANSI/ANS-8.15 value)

Note 1: For ^{237}Np metal, ANSI/ANS-8.15 provides three critical mass estimates for each reflector condition. The first estimate is deduced from reactivity coefficient measurements based on LANL experimental measurements. The second and third estimates are computational results (using differing computational methods) by H. K. Clark (Savannah River Laboratory) and R. M. Westfall (ORNL). The ANSI/ANS-8.15 estimates for $^{237}\text{NpO}_2$ are computed results by H. K. Clark.

Note 2: The density of ^{237}Np metal is assumed to be 20.476 g/cm^3 ; the density of $^{237}\text{NpO}_2$ is assumed to be 11.143 g/cm^3 . These values are in current use by the ANSI/ANS-8.15 Working Group*. The SS304L is modeled with a density of 7.92 g/cm^3 , consisting of 69.5% Fe, 19% Cr, 9.5% Ni, and 2% Mn by weight, with a radial thickness of 20 cm. The stainless steel model is taken from R. M. Westfall's report⁷, "Critical Masses for the Even-Neutron-Numbered Transuranium Actinides."

The "Current Results" of Table 3 compare well with ANSI/ANS-8.15 critical estimates for ^{237}Np metal. The current results for ^{237}Np metal (no reflector and SS304L reflector) are about 7% and 14% greater than Clark's estimates. This difference is comparable to that seen between "Current Results" and Clark's estimates for $^{237}\text{NpO}_2$.

* Internal ORNL Correspondence (electronic mail), John E. Bigelow to distribution, "Computed Actinide Densities," September 19, 1997.

Also, as part of current work, the two ANSI/ANS-8.15 subcritical limits were modeled to estimate the neutron multiplication constants (k_{eff} values) of those limits. For ^{237}Np metal with a stainless steel reflector, the subcritical limit (20 kg ^{237}Np) has a computed k_{eff} value of ~ 0.86 . For $^{237}\text{NpO}_2$ at theoretical density and with a stainless steel reflector, the subcritical limit (90 kg ^{237}Np) has a computed k_{eff} value of ~ 0.88 . The basis of the ANSI/ANS-8.15 subcritical limits for NpO_2 are the critical mass estimates provided in Appendix B of the Standard: the subcritical limits are approximately half of the computed critical mass estimates.

The Standard's subcritical limit value of 90 kg of ^{237}Np as $^{237}\text{NpO}_2$ at theoretical density, with a stainless steel reflector, is considered an adequate subcritical limit for material at theoretical density, based on

- (a) the comparable values of current critical estimates and those given in ANSI/ANS-8.15 Appendix B (the comparison of Table 3, above),
- (b) the conservative basis of the $^{237}\text{NpO}_2$ subcritical limits (half of the critical mass estimates), and
- (c) the current-effort results ($k_{\text{eff}} \sim 0.88$) for the ANSI/ANS-8.15 stainless-steel-reflected subcritical limits.

3.5 THE EFFECT OF OXIDE DENSITIES LESS THAN THEORETICAL

The relationship of the $^{237}\text{NpO}_2$ material density and critical requirements is defined by the "core-density" correlation as described in LA-3612⁸ and LA-10860-MS⁹, as well as many other standard NCS reference handbooks. In that technique, the spherical critical mass at a reference density ρ_0 is designated as M_{co} . At an adjusted density of ρ , the spherical critical mass is M_c . These parameters are related according to the expression

$$\frac{M_c}{M_{co}} = \left(\frac{\rho}{\rho_0} \right)^{-n}$$

While neither critical experiment data nor specific core-density data are available for ^{237}Np , consideration of the core density exponent behavior of ^{235}U and ^{239}Pu may support the range of the core-density exponent n for ^{237}Np .

For an unreflected system, reactor theory predicts that the value of n is exactly 2 for any fissionable material. For a reflected system, in which the reflector does not vary (remains of a constant radial thickness and density), the exponent is generally dependent on the fissionable nuclide, the degree of moderation, and the type of reflector present. For reflected systems, the less important the effect of the reflector, the closer the value of n is to 2. The dependence of n on the effectiveness of various reflectors about unmoderated ^{235}U or ^{239}Pu metal is illustrated by Fig. 3.

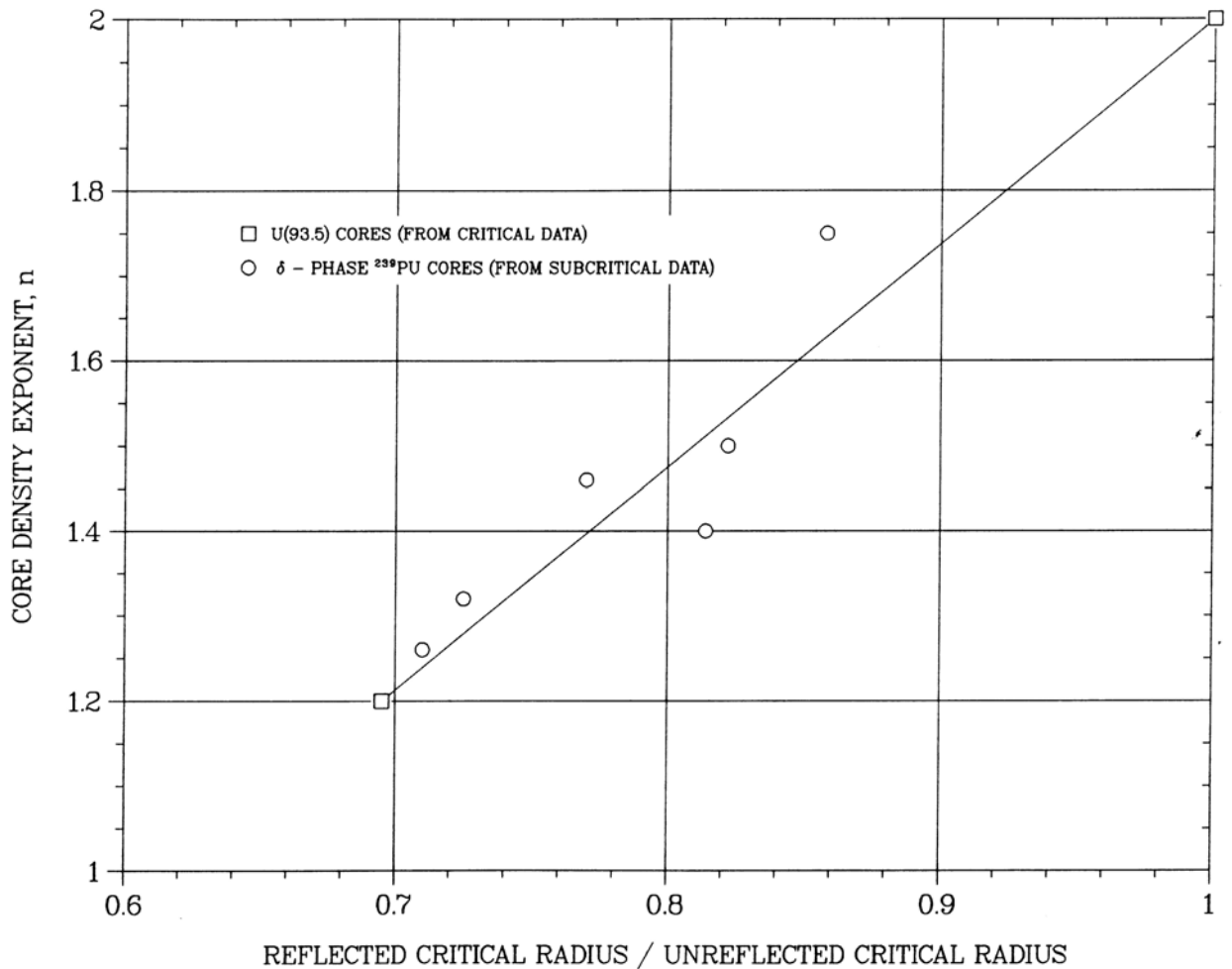


Fig. 3. Density Exponents of Unmoderated Spherical Cores in Constant-Density Reflectors.
Critical Mass = constant (Core Density)⁻ⁿ (Source: Fig. 8 of LA-10860-MS)

Figure 4 provides core-density exponent data from LA-10860-MS, for spheres of ^{239}Pu and ^{235}U as a function of moderation. At very high $\text{H}/^{235}\text{U}$ or $\text{H}/^{239}\text{Pu}$ atom ratios, the fissile material is dilute, and the physical size of the fissile assembly is large. As the moderation ratio further increases, the relative worth of the reflector decreases and n approaches the limiting value of 2.

For unmoderated ^{235}U with a water reflector, $n \sim 1.48$. For unmoderated ^{235}U , the effect of reflector provision is generally significant. LA-10860-MS provides critical mass estimates (based on experimental data) for highly enriched uranium ($\sim 93\%$ ^{235}U enrichment) in metal form, in spherical geometry, for various reflector conditions. In Table 4 below, the LA-10860-MS data for ^{235}U are compared to computed data (from ANSI/ANS-8.15) for $^{237}\text{NpO}_2$ at theoretical density and under similar reflector conditions. It may be seen that the (reflected critical radii/unreflected critical radii) ratios (r/r_c) for $^{237}\text{NpO}_2$ are significantly greater than the corresponding values for ^{235}U metal.

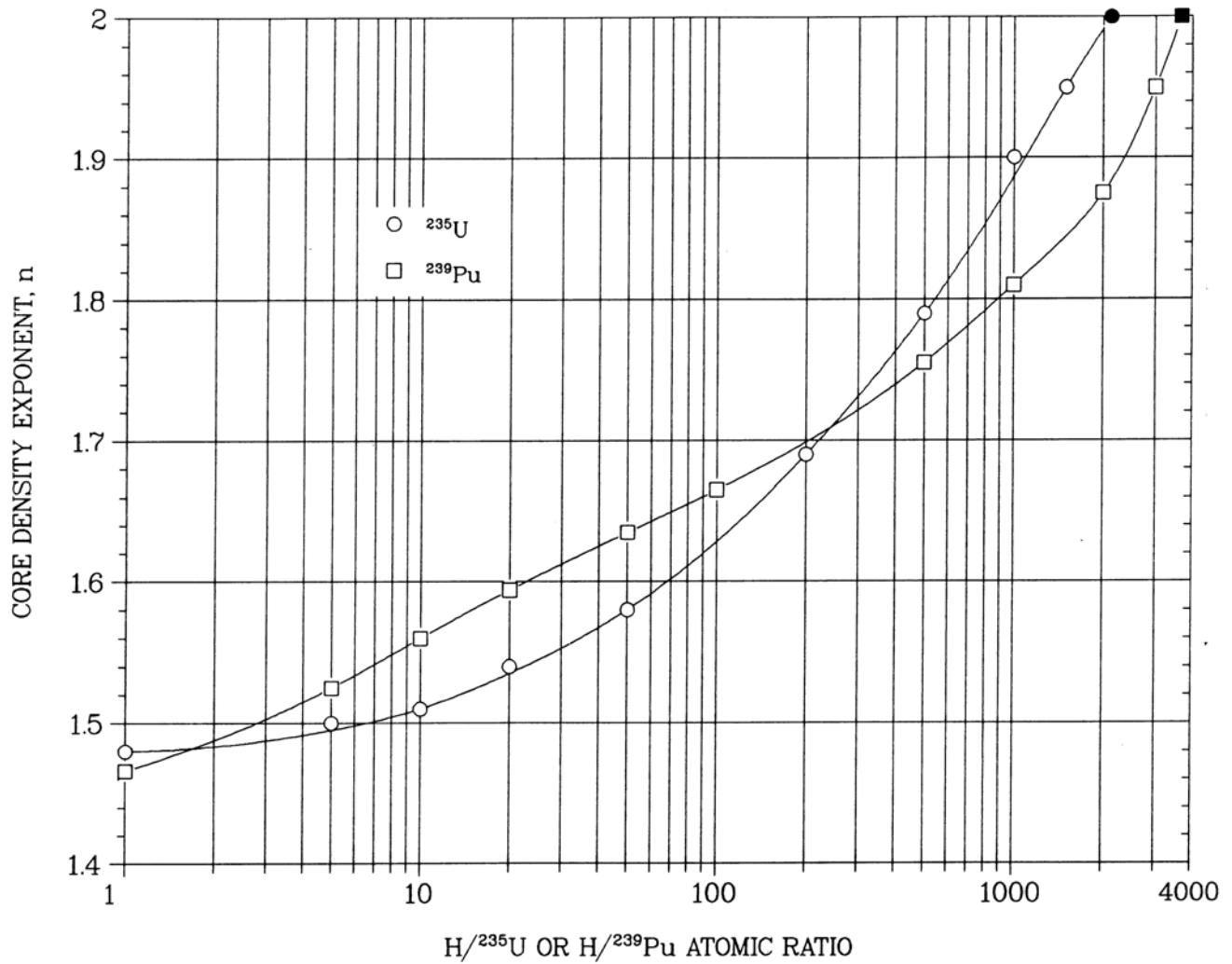


Fig. 4. Calculated Core-Density Exponents for Water-Moderated Spheres of Homogeneous Metal-Water Mixtures.

The solid symbols reflect limiting conditions. (Source: Fig. 9 of LA-10860-MS)

Table 4. Comparison of Reflector Effects for ^{235}U as Highly Enriched Uranium Metal and for $^{237}\text{NpO}_2$, Material in Spherical Geometry at Theoretical Density

^{235}U Data Based on Experiments, Reported in LA-10860-MS

Unreflected Critical Mass	~ 49.1 kg ^{235}U	radius ~ 8.7 cm	(= $r_{\text{u-235u}}$)
Iron Reflected Critical Mass	~ 23.2 kg ^{235}U	radius ~ 6.8 cm	($r/r_{\text{u-235u}} \sim 0.78$)
Water Reflected Critical Mass	~ 22.8 kg ^{235}U	radius ~ 6.8 cm	($r/r_{\text{u-235u}} \sim 0.78$)

$^{237}\text{NpO}_2$ Computed Data as Stated in ANSI/ANS-8.15 Appendix B

Unreflected Critical Mass	~ 288 kg ^{237}Np	radius ~ 19.1 cm	(= $r_{\text{u-237npO2}}$)
Steel Reflected Critical Mass	~ 187 kg ^{237}Np	radius ~ 16.6 cm	($r/r_{\text{u-237npO2}} \sim 0.87$)
Water Reflected Critical Mass	~ 272 kg ^{237}Np	radius ~ 18.8 cm	($r/r_{\text{u-237npO2}} \sim 0.98$)

Based on Fig. 3's dependence of n on r/r_c , and values of r/r_c of Table 4, it appears that the core-density exponent for $^{237}\text{NpO}_2$ should be intermediate to the value of 2 and the core-density exponent for unmoderated ^{235}U . Since the reflector "worth" of iron and water on the ^{235}U metal core are nearly equal ($M_c = 23.2 \text{ kg } ^{235}\text{U}$ for an iron reflector and $M_c = 22.8 \text{ kg } ^{235}\text{U}$ for water reflector), it is reasonable to assume that the unmoderated ^{235}U core density exponent for a water reflector (1.48) is about equal to the core density exponent for an iron reflector. Hence, one would expect the core density exponent for $^{237}\text{NpO}_2$ with a steel reflector to be somewhere in the range of $n = 1.4$ to 2.0.

The significant difference in ^{235}U and $^{237}\text{NpO}_2$ water-reflected r/r_c values of Table 3 results from the fact that ^{235}U is fissile (may fission with reduced-energy neutrons returned by the reflector) whereas ^{237}Np is not fissile. Neutrons migrating from a ^{237}Np assembly into a water reflector must suffer at least one scattering collision in order to reenter the ^{237}Np assembly; an average of about one collision between a fission neutron and a water molecule results in a neutron energy decrease to the ^{237}Np fission threshold. For these reasons, $^{237}\text{NpO}_2$ critical requirements for moderating reflectors should be only slightly less than the unreflected $^{237}\text{NpO}_2$ critical mass requirement. The core density exponent for $^{237}\text{NpO}_2$ with a water (or other type) moderating reflector should be close to $n = 2.0$.

The only type of fissionable material system that may achieve very low core density exponents are "cavity reactors." A cavity reactor employs a moderating reflector of very low neutron absorption capability (e.g., graphite, heavy water, beryllium metal). The "core" region consists of a spherical or cylindrical geometry. The core region is filled with fissile material at a low density (e.g., a gas or matrix) or the cavity interior is provided with a liner of fissile material (in which case most of the core region is void). The core lacks a moderator intermixed with the fissile material; the reflector acts as the moderator. With correctly selected parameters, a system may be established that has a core density exponent of zero or less. [A reduction in fissile density may even result in a reduction in critical mass, a type of reactor system that W. R. Stratton describes as "metastable."⁸] However, ^{237}Np has a fission threshold; moderation of neutrons cannot serve to reduce ^{237}Np critical mass requirements. No viable means exists to achieve either a cavity reactor assembly or a very low core density exponent using ^{237}Np .

Based on the above discussion, a core density exponent value of $n = 1$ is judged applicable (and highly conservative) for use with stainless-steel-reflected $^{237}\text{NpO}_2$ critical data. As an illustration of the level of conservatism in this conclusion, Appendix B (Section B.5) provides critical estimates for $^{237}\text{NpO}_2$ at oxide density fractions of 0.5 and 0.1. Table 5, below, compares these results to previously noted Appendix B estimates for $^{237}\text{NpO}_2$ at theoretical density. From this data, $^{237}\text{NpO}_2$ core density exponents may be deduced.

Table 5. Current Work: Computed Core Density Exponents for $^{237}\text{NpO}_2$
(Summary of data provided in Appendix B, Section B.5)

(ρ/ρ_0)	Calc. Critical Mass, Unreflected		Calc. Critical Mass, Stainless-Steel Refl.	
	(kg ^{237}Np)	n	(kg ^{237}Np)	n
1.0	337	-	216	-
0.5	1350	2.00	776	1.85
0.1	33400	2.00	16500	1.88

Table 5 data notes that the core density exponent for unreflected $^{237}\text{NpO}_2$ spheres is equal to 2, in agreement with theory. The calculated core density exponents for stainless-steel-reflected $^{237}\text{NpO}_2$ spheres (1.85 and 1.88) are within the expected range: greater than the value of n expected for unmoderated ^{235}U ($n \sim 1.4$) and somewhat less than the limiting value of $n = 2$.

Table 5 data is consistent with the prior conclusion that a value of $n = 1$ is conservatively applicable for stainless-steel reflected $^{237}\text{NpO}_2$ spheres.

The core-density relationship is typically applied to a reference critical mass value. However, the core-density exponent technique may reasonably be applied to a reference subcritical mass limit, provided adequate conservatism is applied. For $^{237}\text{NpO}_2$, considerable conservatisms exist in the reference subcritical limit (90 kg of ^{237}Np for a stainless steel reflector, for oxide at theoretical density) and in the selected, conservative core density exponent ($n = 1$).

The primary subcritical limit for $^{237}\text{NpO}_2$ (90 kg ^{237}Np for oxide at theoretical density) may thus be readily adjusted for lower densities. The reduced-density subcritical limit is inversely proportional to the density reduction factor of ρ/ρ_0 . For oxide at half theoretical density, the applicable subcritical limit is 180 kg ^{237}Np . For oxide at 1/10 of theoretical density, the applicable subcritical limit is 900 kg ^{237}Np .

The expected maximum density of the $^{237}\text{NpO}_2$, based on product measurements from the neptunium oxide manufacturing process*, is $\sim 2.5 \text{ g/cm}^3$. This value is based on multiple tap density measurements and appears repeatable. For this material, the density reduction factor $\rho/\rho_0 = 0.224$.

Current computational results of Table 5 cannot be validated due to lack of ^{237}Np critical experiment benchmarks. Based on Table 5 results, the current computation method predicts that for $^{237}\text{NpO}_2$ at a density of 2.5 g/cm^3 , the unreflected critical mass requirement would be $\sim 6700 \text{ kg } ^{237}\text{Np}$, and the predicted steel-reflected critical mass requirement would be $\sim 3400 \text{ kg } ^{237}\text{Np}$.

Since Table 5 results cannot be validated, this assessment employs the conservative ANSI/ANS-8.19 steel-reflected $^{237}\text{NpO}_2$ subcritical limit (90 kg ^{237}Np), adjusted with a conservative core-density exponent of $n = 1$. For $^{237}\text{NpO}_2$ (at a density of 2.5 g/cm^3), the adjusted subcritical mass limit is $\sim 400 \text{ kg } ^{237}\text{Np}$. Provided the oxide density is no greater than 2.5 g/cm^3 , it may be stated that 400 kg of ^{237}Np will remain subcritical without regard as to the material configuration.

* Correspondence (electronic mail), G. Rodrigues (Savannah River Technology Center) to R. M. Wham (ORNL), "Tap Density," July 30, 2003.

4. DOT 9975 CONTAINER DESCRIPTION

The DOT 9975 container presents a robust package for confinement of the $^{237}\text{NpO}_2$. The following descriptions are extracted from Chapter 6 (NCS Evaluation) of the current Safety Analysis Report for Packaging - Packages 9972 - 9975, WSRC-SA-7, Revision 13¹⁰. (This document is referred to as the "current DOT 9975 SARP." The current DOT 9975 SARP does not authorize the needed $^{237}\text{NpO}_2$ loadings; a new or revised SARP must be generated.)

Figure 5 duplicates Fig. 6.12 from the current DOT 9975 SARP, and illustrates the construction of the DOT 9975 container.

The primary containment vessel (PCV) is a 5-inch Schedule 40 stainless steel pipe, provided with a thick plug and locking nut. This item will retain the $^{237}\text{NpO}_2$ oxide, potentially present in food-pack cans, a stainless steel can identified as a "3013" container, or some other type of canister(s) for convenience of handling. Present plans call for up to three food-pack cans per DOT 9975 container, with the total loading of all cans summing to no more than 6 kg ^{237}Np . The PCV is described as meeting pressure vessel design code.

The secondary containment vessel (SCV) is a 6-inch Schedule 40 stainless steel pipe, also designed according to pressure vessel code. A nominal 1/2-inch-thick-lead liner is provided about the SCV to attenuate the gamma radiation from the ^{237}Np payload. Cane fiberboard (Celotex®)* insulation fills most of the remaining capacity of the 35-gallon outer stainless steel drum. Aluminum components may be present as axial spacers (within the PCV, above and below the PCV, within the SCV), and as top and bottom plates located just above and below the SCV. Sleeves of gamma-shielding materials (steel or lead) may be inserted into the annular gap between the payload containers and the PCV, and into the annular gap between the PCV and SCV.

The DOT 9975 SARP notes that the PCV and SCV are shown to remain intact, undamaged as a result of sequential 10-meter (30-ft) drop, puncture, impact, and fire exposure conditions as specified for DOT Type B container testing purposes. For NCS assessment purposes for $^{237}\text{NpO}_2$, even if the PCV and the SCV lose their gas-tight closure, it is improbable that any significant loss of oxide from the vessels would result. To cause significant oxide loss to locations exterior to the SCV, very severe mechanical damage would be required to the PCV, SCV, the stainless steel drum used for the outer DOT 9975 packaging, and to intervening insulation and shielding components.

For purposes of simulating triangular-pitch arrays of DOT 9975 containers using a rectangular array layout, the DOT 9975 SARP employs ~ 7% reduction in the outer diameter of the DOT 9975 container model. (Fig. 5 depicts the actual outer diameter, not the reduced diameter used for the NCS models.) The thickness of the outer stainless steel shell (of the 35-gallon drum) is maintained, and the geometry of the lead shield, the aluminum plates, and the SCV and PCV are not changed. This modeling adjustment has the effect of underestimating the amount of Celotex actually present in each drum. The nominal Celotex volume per DOT 9975 container (as might be deduced from Fig. 5 and SARP descriptions) is ~ 116 liters. For the undamaged-condition NCS model described in the SARP (and employed in Appendix C for DOT 9975 models), the modeled volume of Celotex is only ~ 97 liters.

* "Celotex" is a registered trademark of the Celotex Corporation. "Celotex" is commonly used in the industry as a reference to cane fiberboard insulation, and the term is so used in this report.

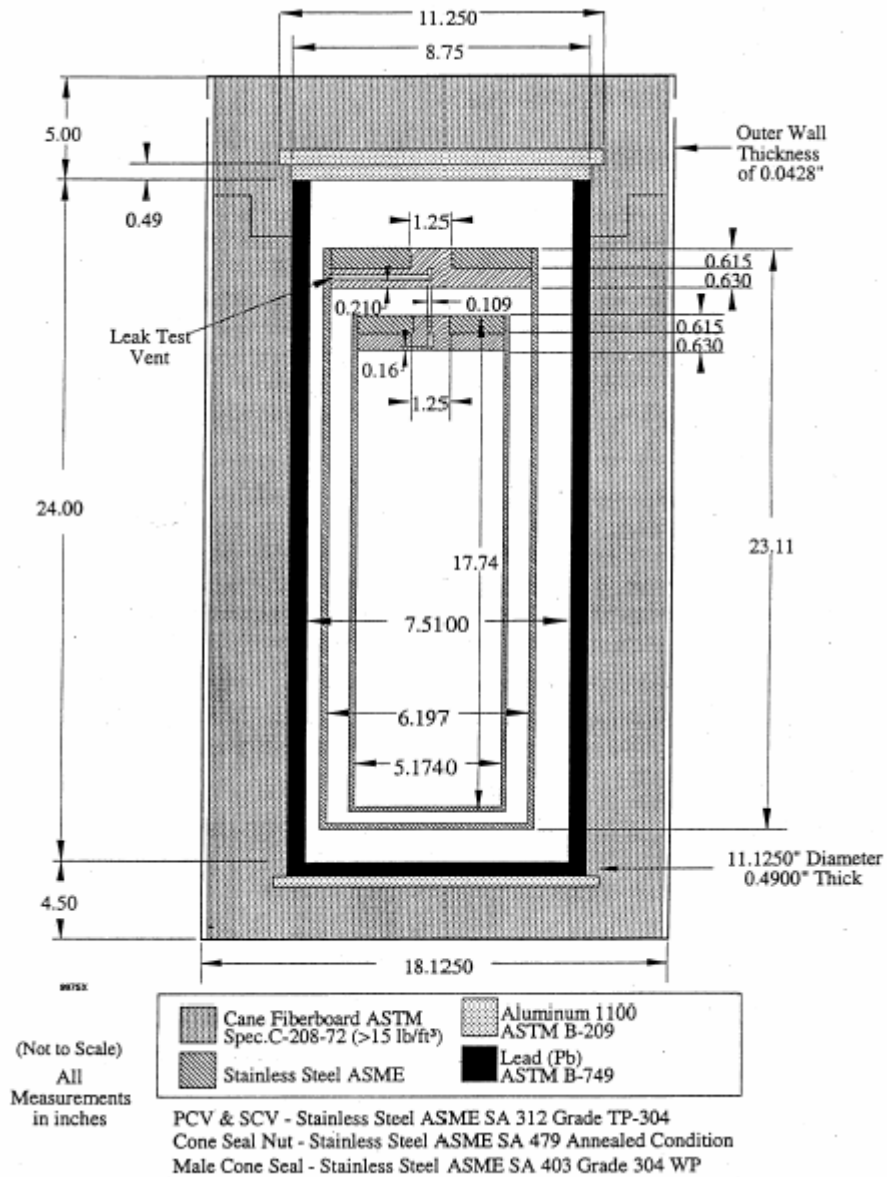


Fig. 5. The 9975 Package Details
 (cross sectional view of vertical cylinder - not to scale).
 (Source: Fig. 6.12 of WSRC-SA-7, Rev. 14)

Figure 6 presents a graphical depiction of the container model, from an NCS code model based on the DOT 9975 SARP description. For Fig. 6, the $^{237}\text{NpO}_2$ payload is modeled as an oxide at half theoretical density, as a cylinder having a height-to-diameter ratio of unity. No inner packaging within the PCV is simulated for the configuration shown by Fig. 6. The actual PCV loading of the DOT 9975 containers will likely consist of one to three stacked food-pack type canisters, with possible inclusion of additional sleeves of shielding material (e.g., lead or steel). The additional shielding sleeve(s) could be installed within the PCV and in the annular gap between the PCV and SCV.

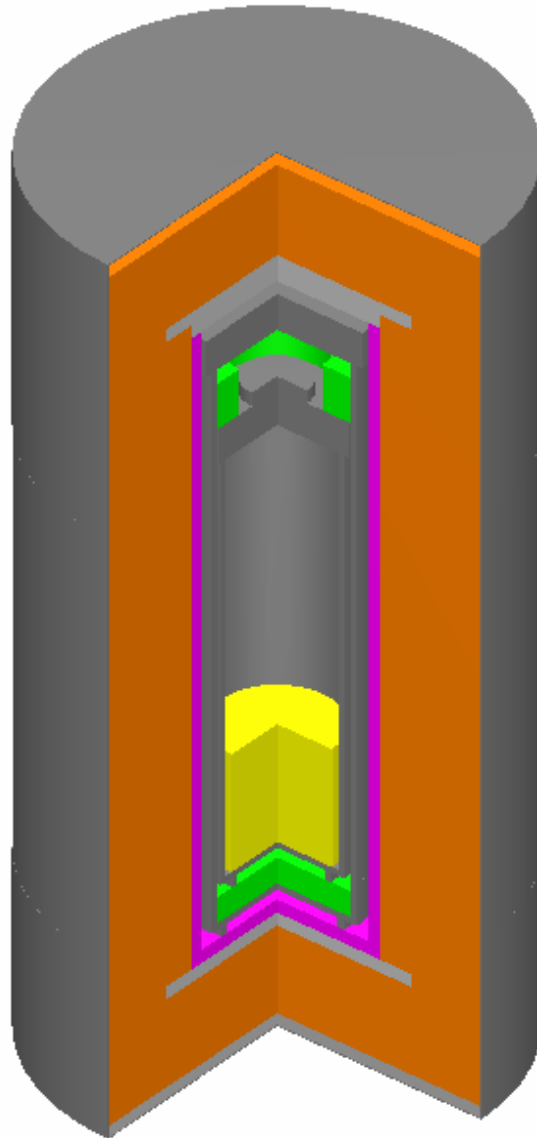


Fig. 6. NCS Model for the DOT 9975 Container with 6 kg ^{237}Np as Oxide at Half Theoretical Density.

(Based on the DOT 9975 SARP NCS Model for an Undamaged Package.
In this graphic, the $^{237}\text{NpO}_2$ payload is modeled as a cylinder with a height-to-diameter ratio of unity.
No inner packaging is included for this configuration within the PCV.)

5. THE CRITICALITY SAFETY OF AN INDIVIDUAL ^{237}Np CONTAINER

A single DOT 9975 container with the maximum loading to be authorized (6 kg ^{237}Np as oxide) is subcritical because the payload is only a small fraction of the ANSI/ANS-8.15 subcritical limit of 90 kg ^{237}Np (as oxide).

The reflector conditions of the package construction (multiple thin layers of steel, lead, surrounded by Celotex at $\sim 0.2 \text{ g/cm}^3$) are bounded by that considered for the ANSI/ANS-8.15 subcritical limit (stainless steel reflector, $\sim 20 \text{ cm}$ thickness, closely fitting about the fissionable material).

No assumption need be made about the oxide density, since the ANSI/ANS-8.15 subcritical limit is based on theoretical density of the oxide.

It is considered unlikely that significantly greater than 6 kg ^{237}Np as oxide might be loaded into an individual DOT 9975 container. Any excess beyond this maximum-approved-loading would presumably require administrative failures on the part of personnel performing $^{237}\text{NpO}_2$ packaging operations. The DOT 9975 SARP NCS model has an internal volume (slight overestimate) for the PCV of 5.56 liters. Since the oxide is expected to have a density $\sim 25\%$ of theoretical and smaller convenience canisters will be used to handle and load the oxide into the PCV, the loading of a DOT 9975 container cannot reasonably exceed $\sim 12 \text{ kg } ^{237}\text{Np}$.

For typical DOT containers loaded with fissionable material, inleakage of water or presence of unintended amounts of hydrogenous packing materials usually represent NCS concerns. Since ^{237}Np has a fission threshold, the most reactive condition is the normal condition (absence of any significant amount of moderator materials within the PCV). Any failures resulting in presence of unanticipated amounts of neutron moderators within the PCV may serve to significantly reduce the k_{eff} value of a single DOT 9975 (if intermixing of moderator material and the oxide payload occurs). If the additional moderator material acts only as a reflector about internally dry canisters of $^{237}\text{NpO}_2$, the reflector condition remains bounded by the ANSI/ANS-8.15 consideration of a 20-cm thick, non-moderating stainless steel reflector.

Should gross material release from a single DOT 9975 container occur, there is no risk of a criticality accident regardless of whether the released material is dispersed or becomes moderated (e.g., the released oxide is contacted by water).

Given that the loading of a single DOT 9975 container is far less than the ANSI/ANS-8.15 subcritical limit of 90 kg ^{237}Np as oxide, and the fact that the ANSI/ANS-8.15 limit is based on worst-case conditions (spherical geometry, theoretical-density oxide with no intermixed moderator, fully reflected by a thick non-moderating reflector), a criticality accident is not a physically possible mishap for a single DOT 9975 container, for normal or credible abnormal conditions.

6. CRITICALITY SAFETY OF ARRAYS OF ^{237}Np CONTAINERS

6.1 NCS BASED ON MODERATION BY INSULATION MATERIALS

Section 3.3 discussed the effect of neutron moderators. It was demonstrated that on average, only about 1 collision of a ^{237}Np fission neutron with a water molecule is required to cause the neutron energy to decrease to near the ^{237}Np fission threshold.

Table 2 predicts that for a uniform mixture of ^{237}Np and hydrogen, $k_{\infty} < 1$ if the H: ^{237}Np atom ratio is ~ 1 or greater. Even a slight amount of hydrogen moderator mixed with ^{237}Np is capable of rendering the fissionable material subcritical regardless of mass, geometry, or reflector conditions.

Significant moderator content (hydrogen) is present in the DOT 9975 insulation material (Celotex). The hydrogen density in the DOT 9975 SARP Celotex model is about 10% of that for full-density water. Consider DOT 9975 containers, each having a payload of 6 kg ^{237}Np as oxide. Each payload represents $\sim 7\%$ of the $^{237}\text{NpO}_2$ subcritical limit (90 kg ^{237}Np) and $\sim 3\%$ or less of the calculated $^{237}\text{NpO}_2$ critical mass requirements (assuming optimum geometry and steel reflection). Therefore, in order for the infinite-system neutron multiplication constant (k_{∞}) to approach unity, significant neutron interaction must exist among the payloads.

Given that each payload represents only a small fraction of critical requirements, neutrons produced in fission may readily migrate from the fissionable material into surrounding regions of Celotex and other container materials of construction. The Celotex is of fairly low density, so that the mean free path of high-energy neutrons in the insulation may be several centimeters. The volume fraction of the array occupied by the $^{237}\text{NpO}_2$ payloads is small. Neutrons migrating through the Celotex find it less probable that a fissionable material volume is encountered; this results in greater neutron track length (and moderation) within the Celotex.

These factors support consideration that the ^{237}Np payloads and the hydrogen moderator of the Celotex are effectively "mixed" to an appreciable extent.

The current SARP model for the DOT 9975 container underestimates the Celotex content as ~ 97 liters; the actual Celotex volume per container is ~ 116 liters. Using the underestimated Celotex volume and the conservatively low Celotex density of the SARP models (0.20 g/cm^3), each DOT 9975 is determined to contain at least 1200 moles of hydrogen. For a payload of 6 kg ^{237}Np , this results in a DOT 9975 "container average" H: ^{237}Np atom ratio greater than 47. Even considering that the neptunium oxide and the insulation are not homogeneously mixed, it is evident that interaction of the $^{237}\text{NpO}_2$ payloads should be strongly inhibited, or even precluded, by presence of hydrogen in the Celotex.

Even if the "damaged" container model of current SARP were considered (with hydrogen loss due to heat charring of the outer layer of Celotex from the DOT fire exposure test), more than a third of the hydrogen present in the initial, undamaged Celotex remains.

From these observations, it is concluded that an infinite array of DOT 9975 containers, loaded with up to 6 kg ^{237}Np per container in the form of oxide, should be subcritical due to the hydrogen content of the insulation. This conclusion should remain applicable to "damaged" packages, for which some loss of the exterior Celotex is a presumed effect of fire exposure.

In Appendix C, the current SARP NCS model for undamaged DOT 9975 containers (with a 7% outer diameter reduction for rectangular-to-triangular-pitch array equivalency) is employed to compute both single-unit and infinite-array neutron multiplication constants, k_{eff} and k_{∞} values, for $^{237}\text{NpO}_2$ -loaded DOT 9975 containers. Appendix C calculations consider a maximum approved loading per container of 6 kg ^{237}Np as oxide. Material densities of 100%, 50%, and 25% of theoretical density are considered.

The single-unit results (single DOT 9975 container) are only slightly greater than the results for completely unreflected payloads (inner package without the surrounding DOT 9975 container). The container construction provides minimal return of high-energy neutrons into the fissionable material payload.

When Appendix C single-unit results (for an individual DOT 9975 container) are compared to the corresponding infinite-array results, little difference in computed k_{eff} values is seen. The DOT 9975 construction, coupled with the fission-threshold behavior of ^{237}Np , act to neutronically isolate the container payloads.

Because of neutronic isolation of the container payloads, the array k_{eff} values are essentially equal to the single-unit k_{eff} values, and both are controlled by the mass and configuration of an individual payload. To maximize the k_{eff} value of an individual container, the payload should be (a) at maximum (theoretical) density, (b) in the most compact geometry possible, (c) with as much additional steel or lead shielding material as may physically fit within and around the PCV and SCV, and (d) with maximum fissionable material loading.

The most compact geometry models were (a) sphere, (b) a cylinder with height-to-diameter ratio of 1, and (c) a cylinder with radius equal to the PCV. These payload geometry models were employed (as permitted by the NCS models for the payload and the PCV) with preference to the listed sequence.

For possible inclusion of gamma-shielding components within the DOT 9975, it is assumed that the shield material would be stainless steel or lead, with the most likely locations being within the PCV and within the annulus between the PCV and SCV. Appendix C NCS models include replacement of void volumes in these regions with either steel or lead. Also, replacement of the low-density aluminum impact absorbers (located axially between the PCV and SCV) with steel or lead shielding was simulated. Even with non-realistic inclusion of lead or steel throughout these regions, only a slight k_{eff} increase occurred. This appears to be due to increased neutron reflection of an individual payload; no enhanced interaction of containers resulted due to these shielding configuration changes.

For presence of neutron-reflecting materials external to the DOT 9975 container, the container NCS model of Appendix C is insensitive to the condition of external reflection. Unreflected, water-reflected, and concrete-reflected conditions were considered, with no appreciable difference in results.

When the base infinite array NCS model of Appendix C (case c10) was altered to remove 90% of the Celotex, the computed array k_{eff} increase was less than $\Delta k_{\text{eff}} = 0.04$. Only a small fraction of the Celotex appears adequate to preclude interaction of the $^{237}\text{NpO}_2$ payloads.

When the base infinite array NCS model of Appendix C was altered to increase the container payload from 6 kg ^{237}Np to 12 kg ^{237}Np , the computed array k_{eff} increase was less than $\Delta k_{\text{eff}} = 0.04$. Even a 12 kg ^{237}Np "double-batch" loading represents a small fraction of individual-unit ^{237}Np critical mass requirements.

Even with these various conservative considerations, the maximum computed k_{eff} value of Appendix C, for any DOT 9975 container or array configuration, did not exceed 0.5.

An unlimited array of DOT 9975 containers, with a loading limit of 6 kg ^{237}Np as oxide per container, will remain subcritical due to the hydrogen inherent in the package construction. The individual loadings per container are only a small fraction of individual-unit critical mass requirements, and the hydrogen functions as an isolating material to preclude neutron interaction.

6.2 NCS BASED ON LIMITED EFFECTIVE DENSITY OF THE $^{237}\text{NpO}_2$

The outer layer of the DOT 9975 container is comprised of a 35-gallon drum. Based on the dimensions of Fig. 5, the overall drum volume (assuming the displacement of the outermost right circular cylinder) is ~ 142 liters. Based on the actual NCS model for the DOT 9975 container, the (underestimated) overall drum volume is ~ 125 liters.

Within a triangular-pitch array of close-packed cylinders, the void volume between the cylinders represents a volume fraction of about 0.09. This void space is conservatively ignored.

If a loading of 6 kg ^{237}Np per DOT 9975 is considered, and the overall drum displacement is underestimated as 125 liters, the array-average density of ^{237}Np is ~ 0.048 kg ^{237}Np /liter. This represents a density reduction ratio (ρ/ρ_0) of 0.0049 relative to the theoretical-density oxide. A conservative mass increase factor of ~ 200 is obtained using a core density exponent of 1. When applied to the 90 kg ^{237}Np subcritical limit of ANSI/ANS-8.15, the adjusted subcritical mass limit is ~ 18 metric tons of ^{237}Np as oxide.

The core-density technique assumes uniform reduction of the fissionable material without intermixing of other materials with the fissionable materials. However, the individual-container loadings of 6 kg ^{237}Np are but small fractions of single-unit critical requirements. Provision of intervening metallic components fabricated of aluminum, steel or lead should interfere with effective neutron interaction of the small payload masses, but could affect the degree of neutron reflection afforded to each payload. The important effect of hydrogen in the Celotex need not be credited if the overall array density-reduction factor is considered.

A value of 500 kg of ^{237}Np was informally identified as the maximum inventory requiring consideration by this NCS assessment. This inventory (500 kg of ^{237}Np) is only a small fraction of critical requirements (> 18 metric ton estimate above) based simply on the per-container maximum loading (6 kg ^{237}Np) and the volume occupied per DOT 9975 container (assumed to be at least 125 liters).

To further illustrate the significant effect of reduced-effective-density of the $^{237}\text{NpO}_2$, consider the volume displaced by the SCV. For this purpose, the current SARP NCS model is used to approximate the SCV dimensions. From Fig. 6.13 of WSRC-SA-7, the outer radius of the SCV model is 8.414 cm (corresponds to the outer diameter of a 6-inch Schedule 40 pipe, 6.625-inches) and the overall height is 58.568 cm (23.1-inches). This yields a displacement volume for the SCV (as a right circular cylinder) of 13.0 liters. With a loading of 6 kg ^{237}Np per SCV, the density reduction factor is ~ 0.05. The inverse of this value gives a conservative mass increase factor of ~ 20. The adjusted subcritical limit is

$$20 (90 \text{ kg } ^{237}\text{Np}) = 1800 \text{ kg } ^{237}\text{Np}.$$

A compact accumulation of DOT 9975 secondary containment vessels, loaded with 6 kg ^{237}Np as oxide each, has a subcritical limit of 1800 kg ^{237}Np . Even considering the evaluation basis of 500 kg ^{237}Np , all DOT 9975 containers could be opened, the SCVs retrieved, and the SCVs compactly accumulated without potential for a nuclear criticality accident. This implies that damage to the outer regions of the DOT 9975 container (e.g., natural-phenomenon-induced distortion of the outer drum and compaction of insulation) will not invalidate the conclusion of subcriticality based on the low effective density of the $^{237}\text{NpO}_2$.

6.3 NCS BASED ON LIMITED MASS (INDIVIDUAL TRANSPORT OPERATIONS)

For purposes of the revised SARP that will cover shipment of $^{237}\text{NpO}_2$ in the DOT 9975, the above logic of Section 6.1 (Celotex moderator acts as a neutron isolator) could be used to support a "criticality index" value of zero for each package. However, to accomplish DOT transport of the $^{237}\text{NpO}_2$, a criticality index of zero is not necessarily required.

For example, the 90 kg ^{237}Np subcritical limit may be viewed as an always-safe mass of ^{237}Np in oxide form. In consideration of the hypothetical accident conditions imposed for DOT fissionable material container design purposes, a mass of 90 kg ^{237}Np remains subcritical independent of package performance. The DOT criticality index per package could be assigned as the quotient of the package loading (kg of ^{237}Np) divided by the subcritical limit of 90 kg ^{237}Np , multiplied by 100. This technique could result in individual-package criticality index assignments greater than 6.0, and transport-vehicle criticality index summations approaching 100. While non-zero criticality indices are viewed by many as indicating some criticality accident potential, control of each shipment to no more than the ANSI/ANS-8.15 subcritical limit of 90 kg ^{237}Np effectively renders a nuclear criticality accident impossible during normal or abnormal conditions of transport.

For on-site shipments, criticality safety may likewise be assured by simply limiting each transport operation to no more than a total of 90 kg of ^{237}Np .

6.4 NCS OF MATERIAL RELEASES

The maximum mass per DOT 9975 container (6 kg ^{237}Np) is only a small fraction of the ANSI/ANS-8.15 steel-reflected limit for $^{237}\text{NpO}_2$ (90 kg ^{237}Np , for material at theoretical density). Consider some accident that is adequately severe to cause breach and bulk release of oxide from more than one $^{237}\text{NpO}_2$ -loaded DOT 9975 container.

The expected tap density of the oxide is $\sim 2.5 \text{ g/cm}^3$. The ANSI/ANS-8.15 limit (steel-reflected conditions) may be conservatively increased to a limit of 400 kg ^{237}Np based on this material density. Thus, the contents of far more than eight $^{237}\text{NpO}_2$ -loaded DOT 9975 containers must be released and compactly accumulated before a criticality risk might result.

The same conclusion applies to $^{237}\text{NpO}_2$ releases near HEU storage containers. If the released oxide is dispersed to a low density, non-compact geometry, the oxide cannot effectively multiply neutrons. If the oxide release is compactly reconfigured adjacent to one or two HEU containers, a criticality accident will not result. The $^{237}\text{NpO}_2$ content of eight DOT 9975 containers represents only a small fraction of $^{237}\text{NpO}_2$ critical requirements for material at the expected density; any arrangement of this material inventory lacks significant neutron multiplication ability. For material disruption and release scenarios, there should be no risk of a criticality accident unless the HEU is reconfigured to a condition adequate to support a criticality accident independent of presence of nearby $^{237}\text{NpO}_2$ materials.

7. CRITICALITY SAFETY OF COMMINGLED STORAGE OF ^{237}Np CONTAINERS AND CONTAINERS OF HIGHLY ENRICHED URANIUM

7.1 EXPECTED EFFECT OF DOT 9975 CONTAINERS ON HEU STORAGE

This section addresses the possible operational need to store the DOT 9975 containers in highly enriched uranium (HEU) storage areas. Of interest is whether the HEU and the ^{237}Np materials may sufficiently interact, so as to reduce the amount or configuration of HEU required to attain critical conditions.

Section 6.1 of this report demonstrates that infinite arrays of DOT 9975 containers may be shown subcritical based on neutron isolation of the individual ^{237}Np payloads (due to neutron moderation provided by the Celotex). This implies that neutrons from other sources external to a DOT 9975 container (or DOT 9975 container array) will likewise not be effective in production of fission neutrons within the $^{237}\text{NpO}_2$ payload(s). Hence the extent of productive neutron interaction between $^{237}\text{NpO}_2$ -loaded DOT 9975 containers and external fissionable materials should be very limited.

The outer layers of each DOT 9975 container consist of Celotex at low density ($\sim 0.2 \text{ g/cm}^3$). Most likely, the primary influence of the DOT 9975 containers on the k_{eff} value of nearby HEU materials is that of a weak neutron reflector, as provided by the packaging materials of construction. It is expected that ordinary concrete ($\sim 2 \text{ g/cm}^3$ or more, normally present as floor and wall construction) is a more effective neutron reflector than the DOT 9975 containers.

7.2 COMPUTATIONAL CHECK FOR INTERACTION OF DOT 9975 CONTAINERS AND HEU

Appendix D provides NCS models and computational results for critical experiments involving HEU cylinders ($\sim 21 \text{ kg U/cylinder}$) in $2 \times 2 \times 2$ arrays, as described in Y-DR-83¹¹ and Y-DR-109¹². The arrays had either concrete or polyethylene reflectors on all six sides. For the selected experiments, the unit cells for each HEU cylinder contained void (air), Celotex, vermiculite, or wood. The intent of these experiments was to simulate interaction of neutrons through low-density moderating materials typical of shipping container construction. The good agreement of Appendix D results with expected $k_{\text{eff}} \sim \text{unity}$ indicates that high-energy neutron scattering and moderation within low-density shipping container insulation materials can be reasonably modeled with the described computational method.

In Appendix E, a fiducial mixed-storage array model is established. The base model for the mixed storage array includes a $7 \times 7 \times 2$ high array of DOT 9975 containers, adjacent to a $6 \times 6 \times 3$ array of HEU metal spheres (20 kg ^{235}U mass each, 100% ^{235}U enrichment).

The DOT 9975 containers were modeled with the same container and payload model of case c01 of Appendix C; the container payload is a theoretical-density sphere of $^{237}\text{NpO}_2$. The payload model is extremely conservative in two regards: (1) the use of the maximum crystalline density as the bulk density of the oxide, and (2) use of a single payload item per DOT 9975 (two or three payload items are expected to be stacked within each DOT 9975). A total of 98 containers (6 kg ^{237}Np each as oxide, $\sim 600 \text{ kg } ^{237}\text{Np}$ total) was modeled in the $7 \times 7 \times 2$ DOT 9975 array.

The HEU storage array was proximate to the +x face of the DOT 9975 array. Each 20 kg U sphere was centered within a 50.8 cm (20-inches) void cuboid. The void cuboid simulates containers designed of metal framework or sheet metal that may compact under severe mechanical force. The steel of such containers is omitted from the NCS models. Intervening packaging and insulation materials (such as Celotex) are not modeled for the HEU containers. The "normal" condition HEU array consisted of a 6 x 6 x 3 array of 108 units.

The vault interior dimensions were modeled as 609.6 cm by 609.6 cm by 304.8 cm tall (20-ft by 20-ft by 10-ft tall). All six faces of the vault were modeled as 60 cm (24-inches) of "Magnuson's concrete" ("MGCONCRETE" as provided by the SCALE 4.4a premixed material library).

The computed k_{eff} value for this "normal" condition of array storage is ~ 0.91 .

The spacing of the HEU units (6 x 6 x 3 array of 108 units) was reduced to ~ 33 cm (~ 13 -inches) so that the computed array k_{eff} value increased to ~ 1.00 . Compared to the normal array condition, the per-unit volume for the HEU units has been reduced to $\sim 27\%$ of its initial condition. If possible, such reconfiguration of a very large number of HEU storage containers would require a severe facility event (e.g. natural phenomenon) as an initiating event.

For the compacted 6 x 6 x 3 HEU array, the computed array $k_{\text{eff}} \sim 1.00$ was found to be independent of whether the immediately adjacent array of DOT 9975 containers were loaded or empty. The array k_{eff} value with loaded DOT 9975 containers only (no HEU units in model) was less than ~ 0.5 . The computed k_{eff} value for the DOT 9975 array is essentially equal to the individual DOT 9975 container k_{eff} value.

The HEU array was reduced in size to a 3 x 3 x 3 array of 27 units on ~ 24 cm (~ 9.5 -inches) centers, corresponding to near-critical conditions. The array was maintained proximate to the DOT 9975 container array. The center spacing represents a cell volume (average array volume per HEU unit) that is $\sim 10\%$ of the "normal" array condition. Such a reconfiguration of a large number of HEU items, if possible, would require some severe, unlikely off-normal facility event. For this lesser-size HEU array, the array k_{eff} value was found to be independent of whether the DOT 9975 containers were loaded or not.

Finally, a 2 x 2 x 2 array of HEU units was considered, with a center spacing of ~ 17 cm (~ 6.75 -inches). This model considers that a hypothetical HEU accident might involve a small number of units. Again, the criticality condition of the fiducial HEU accumulation was found to be independent of whether $^{237}\text{NpO}_2$ was present in the adjacent DOT 9975 container array.

For each of the three critical HEU arrays considered, replacement of the $^{237}\text{NpO}_2$ -loaded DOT 9975 array (~ 600 kg ^{237}Np total) with a concrete wall resulted in computed k_{eff} increases for the HEU arrays of $\Delta k_{\text{eff}} \sim 0.03$. Neutron-reflecting facility structural features (floor and walls as commonly present for storage vaults) provide a more significant contribution to HEU array k_{eff} values than presence of adjacent $^{237}\text{NpO}_2$ -loaded (or empty) DOT 9975 containers.

8. ABNORMAL CONDITIONS AND EVENTS THAT ARE BOUNDED BY THE CRITICALITY SAFETY CONSIDERATIONS

This section summarizes abnormal conditions or events that are considered to be bounded by this criticality safety assessment:

Storage

- (1) Overload of multiple DOT 9975 containers. Double-batching (overload of all containers to 12 kg ^{237}Np /container), should not affect any NCS conclusions for subcriticality. This off-normal condition is not considered a realistic possibility if appropriate procedural control exists for loading operations.
- (2) Any increase in reflection to DOT 9975 storage arrays (e.g., water-flooding, collapse of roof onto array).
- (3) Any unintended presence of hydrogen moderator (e.g., roof leak, fire sprinkler activation).
- (4) Facility fire. A facility fire might damage Celotex and cause hydrogen loss from the Celotex, but not all hydrogen would be removed from the container. The array-average material density would remain very low compared to typical oxide densities.
- (5) Explosion or severe mechanical impact. Burst of a propane tank on a forklift could cause damage to several containers; some failure involving an overhead crane might result in a heavy load drop onto DOT 9975 containers.
Breach and full rupture and material release from as many as eight DOT 9975 containers (coupled with unlikely reconfiguration of the released materials) would not present a criticality accident risk.
- (6) High winds, tornados, and seismic events. Such events may potentially cause damage to multiple DOT 9975 containers. However, the damage would generally be limited to the outer layers of container construction. Gross decrease in the overall container volume is not expected. Even if the secondary containment vessels (pressure vessels) are removed from all DOT 9975 containers in storage and compactly accumulated, critical conditions would not be achieved; this condition bounds any situations where significant damage to outer layers of packaging may occur. Breach and full rupture and material release from as many as eight DOT 9975 containers would not present a criticality risk.

Handling

- (7) Handling errors for individual DOT 9975 containers or pallets of DOT 9975 containers. Errors resulting in damage to the container exterior are of no NCS relevance (e.g., compaction or puncture of outer drum or Celotex insulation). Errors involving severe mechanical damage (puncture or rupture) to both the PCV and SCV are considered as credibly affecting a few containers. As many as eight DOT 9975 containers may be breached, fully releasing their content of $^{237}\text{NpO}_2$, without significantly approaching a released-material inventory comparable to the ANSI/ANS-8.15 subcritical limit of 90 kg ^{237}Np .

Transport

- (8) Any type or extent of transport vehicle accident, assuming up to 90 kg ^{237}Np per transport operation. (This applies to both DOT and on-site transport, regardless of whether the Certificate of Compliance for the DOT 9975 remains active beyond initial use.)

9. CONCLUSION

A nuclear criticality safety assessment for the DOT 9975 container, with $^{237}\text{NpO}_2$ loadings, has been performed. The assessment concludes that there is no viable potential for a nuclear criticality accident for storage, handling, and transport operations involving closed DOT 9975 containers, under normal or credible abnormal conditions.

The technical bases for this conclusion include:

1. The ^{237}Np loading per container is only a small fraction of the very conservative single-unit subcritical mass limit for $^{237}\text{NpO}_2$ as identified by ANSI/ANS-8.15-1981. The total inventory of ^{237}Np available to activities covered by this report does not exceed 500 kg ^{237}Np .
2. The internal payload volume per container is small relative to the overall volume of each shipping/storage container. Due to the nature of construction of each container, the overall volume of each container cannot be significantly reduced due to severe facility events (e.g., seismic or high wind events, major facility fire). These factors result in a $^{237}\text{NpO}_2$ density (volumetric average over the array) that is a small fraction of the actual oxide density.
3. The shipping container design incorporates a packaging and insulation material (Celotex) that functions as a neutron moderator due to its hydrogen content. When subjected to neutron-moderated conditions, ^{237}Np cannot support a nuclear criticality accident. Presence of Celotex as an integral packaging material also mitigates neutron interaction between the ^{237}Np payload materials and other fissionable materials (e.g., highly enriched uranium) that may be handled or stored in areas adjacent to the DOT 9975 containers.

The essential administrative and design factors supporting this NCS conclusion are as follows:

1. The loading per individual shipping/storage container will not exceed 6 kg ^{237}Np as NpO_2 . The total ^{237}Np inventory will not exceed 500 kg. Pu and U isotopes may be present, but the total Pu plus U content will not exceed 1% of the neptunium weight.
2. Each shipping/storage container will be a container constructed according to DOT 9975 design specifications (expiration of the DOT Certificate of Compliance is not a factor).
3. No operations will be conducted that involve planned opening of the shipping/storage containers.

Once the DOT 9975 containers are loaded and prepared for DOT transport, the first two NCS factors above (contents per container and the design of the container) are reasonably assured for all subsequent closed-container activities. This assurance exists without need for formal administrative specifications (such as a specific Technical Safety Requirement, TSR) for container design. It is reasonable to assume that site-to-site material transfers will include transfer of appropriate documentation, so that organizations subsequently responsible for the material have assurance that the fissionable material loading per container and the container construction are known.

This NCS conclusion does not apply to operations associated with removal of multiple inner packages from the DOT 9975 containers, such as when the DOT 9975 containers will be unloaded at ORNL.

Control of operations to preclude unauthorized unloading of the DOT 9975 containers should not generally warrant consideration as an explicit TSR commitment. For off-site transport activities, the packages must remain closed to remain in compliance with DOT transport requirements. For on-site transport activities, a transportation safety document and TSR will provide approval that is clearly limited to transport of closed containers. For storage within DOE facilities, the Facility Authorization Basis (FAB) documents would be expected to have a limited approval scope for facilities providing closed container storage only. Typical facility, transport, or material control management systems should be adequate to prevent unauthorized DOT 9975 container unloading activities.

This assessment is considered to be an adequate judgment basis to decide, as required by ANSI/ANS-8.3-1997 *American National Standard Criticality Accident Alarm*¹³, whether criticality alarm coverage is deemed necessary.

The primary NCS conclusion of the assessment may be stated as follows:

Once the DOT 9975 containers are properly constructed and loaded, subsequent closed-container processes (storage, handling, and transport of closed containers only) may be considered critically safe by nature of process.

Where those processes involve closed ²³⁷NpO₂-loaded DOT 9975 containers separate from any other fissionable materials, provision of criticality accident alarm coverage is not warranted. (Criticality accident alarm coverage may exist or may be required if significant inventories of other fissionable materials are stored, handled, or transported with the DOT 9975 containers.)

This conclusion includes assumption that extremely improbable events (e.g., explosion, forklift puncture of container, severe transport accident) may cause release of ²³⁷NpO₂ from some limited number of directly affected containers. Potential release of oxide from as many as eight DOT 9975 containers (coupled with unlikely compact reconfiguration of the oxide) does not challenge this NCS conclusion.

REFERENCES

1. ANSI/ANS-8.15-1981 (R1995), *American National Standard Nuclear Criticality Control of Special Actinide Elements*, American Nuclear Society, La Grange Park, Illinois, 1981.
2. ANSI/ANS-8.1-1998, *American National Standard Nuclear Criticality Safety in Operations with Fissionable Materials Outside Reactors*, American Nuclear Society, La Grange Park, Illinois, 1998.
3. CCC-701/MCNP4C2, *MCNP 4c2, Monte-Carlo N-Particle Transport Code System*, available on MCNP 4c2 distribution CD.
4. NUREG/CR-0200, Rev. 6 (ORNL/NUREG/CSD-2/R6), *SCALE, A Modular Code System for Performing Standardized Computer Analyses for Licensing Evaluation*, March 2000.
5. John R. Lamarsh, Nuclear Reactor Theory, Addison-Wesley Publishing Company, 1966.
6. Arthur R. Foster and Robert L. Wright, Jr., Basic Nuclear Engineering, Second Edition, Allyn and Bacon, Inc., 1973.
7. R. M. Westfall, "Critical Masses for the Even-Neutron-Numbered Transuranium Actinides," *Nucl. Sci. Eng.*, 79, 237 (1981).
8. W. R. Stratton, "Criticality Data and Factors Affecting Criticality of Single Homogeneous Units," LA-3612, Los Alamos Scientific Laboratory, 1964.
9. H. C. Paxton and N. L. Pruvost, "Critical Dimensions of Systems Containing ^{235}U , ^{239}Pu , and ^{233}U ," 1986 Revision, LA-10860-MS, Los Alamos National Laboratory, 1987.
10. Chapter 6, Nuclear Criticality Safety Evaluation, of "Safety Analysis Report for Packaging, Packages 9972 - 9975," WSRC-SA-7, Revision 14, Westinghouse Savannah River Company, Aiken, SC 29808.
11. D. W. Magnuson, "Critical Three-Dimensional Arrays of Neutron Interacting Units: Part III Arrays of U(93.2) Metal Separated by Various Materials," Y-DR-83, Union Carbide Corporation, Oak Ridge Y-12 Plant, 1972.
12. D. W. Magnuson, "Critical Three-Dimensional Arrays of Neutron Interacting Units: Part IV Arrays of U(93.2) Metal Reflected by Concrete and Arrays Separated by Vermiculite and Reflected by Polyethylene," Y-DR-109, Union Carbide Corporation, Oak Ridge Y-12 Plant, 1973.
13. ANSI/ANS-8.3-1997, *American National Standard Criticality Accident Alarm*, American Nuclear Society, La Grange Park, Illinois, 1997.
14. Nuclides and Isotopes, Fifteenth Edition (Chart of the Nuclides), General Electric Company and Knolls Atomic Power Laboratory, 1996.

APPENDIX A
SCOPING COMPUTATIONS FOR k_{∞} FOR ^{237}Np -H₂O MIXTURES

APPENDIX A. SCOPING COMPUTATIONS FOR k_{∞} FOR ^{237}Np -H₂O MIXTURES

A.1 Introduction

This appendix provides NCS calculations that estimate the infinite-system neutron multiplication factor (k_{∞}) for idealized homogeneous mixtures of water and ^{237}Np metal or mixtures of water and $^{237}\text{NpO}_2$.

These computations are considered to be "scoping" calculations since ^{237}Np critical experiment data is not available to quantitatively validate the computational results. These scoping calculations are used to qualitatively inspect the behavior of ^{237}Np under slightly moderated conditions, and to support prior conclusions (in the body of this report) regarding the criticality physics of ^{237}Np in the presence of small amounts of hydrogen moderator.

A.2 Computational Methods

All calculations were performed in July and August 2003 on a Digital AlphaStation DS10 with a EV67/600 617-MHz central processor unit. The workstation operating system was Compaq Tru64 UNIX, version 5.1 (Rev. 732). The workstation (*ossws5*) was accessed over the ORNL internal Ethernet network as *ossws5.ornl.gov*. Throughout this work, the computer was maintained under the administrative control of the Nuclear Criticality Safety Group of the Operational Safety Services Division of ORNL.

One computational method employed was use of the KENO-V.a Monte Carlo code. The modules for use of KENO-V.a were obtained from a computational software package referred to as SCALE (Standardized Computer Analyses for Licensing Evaluation)⁴. This software package was developed by the Computational Physics and Engineering Division (now part of the Nuclear Science and Technology Division) of the Oak Ridge National Laboratory. The SCALE control sequence CSAS25 was utilized. This control sequence invokes multigroup cross-section processing codes BONAMI and NITAWL prior to execution of KENO-V.a. The neutron cross section library employed was the 238-neutron-energy-group SCALE library, which is based primarily on Evaluated Nuclear Data File/B-V (ENDF/B-V) data.

The second computational method employed was use of the MCNP 4c2 Monte Carlo code. This code is maintained by the Los Alamos National Laboratory. MCNP-supplied continuous-energy neutron cross section data based primarily on ENDF/B-V was used.

SCALE Version 4.4a and MCNP 4c2 were initially installed on *ossws5* in April 2002. Quarterly re-verifications have been routinely performed since then, with no detected problems. The most recent quarterly re-verifications were performed on March 28 and July 4, 2003.

A.3 SCALE 4.4a NCS Model

The NCS geometry model for all cases of this appendix consisted of a cuboid of edge dimension 100 cm. Mirror boundary conditions were imposed on all six faces of the cuboid to simulate a geometrically infinite system.

For an infinite system, k_{∞} is independent of the mixture material density. All NCS material models of this appendix assumed a fiducial ^{237}Np density of 9.817720 g/cm^3 . (This selected value happens to correspond to the ^{237}Np density for $^{237}\text{NpO}_2$, when the oxide is present at theoretical density.) The corresponding input ^{237}Np atom density for all SCALE runs was $N_{^{237}\text{Np}} = 2.4942 \times 10^{-2} \text{ a/bn-cm}$. This atomic density value is derived using isotopic weights and Avogadro's number as provided by Nuclides and Isotopes, Fifteenth Edition¹⁴.

For $^{237}\text{Np-H}_2\text{O}$ mixtures, the specified hydrogen density was equal to the product of the desired H: ^{237}Np atom ratio and the ^{237}Np atom density. The oxygen atom density for water was set to half of the hydrogen atom density. For $^{237}\text{NpO}_2\text{-H}_2\text{O}$ mixtures, the hydrogen and oxygen atom density specifications for H_2O were not changed. An incremental oxygen atom density (equal to twice the ^{237}Np atom density) was specified to simulate that oxygen present in the oxide. [Note: The computed values of k_{∞} are independent of whether physical mixtures of $^{237}\text{Np-H}_2\text{O}$ or $^{237}\text{NpO}_2\text{-H}_2\text{O}$ may exist at these described mixture densities. The only factor determining k_{∞} for these mixtures are the proportions (atom ratios) of hydrogen and oxygen to ^{237}Np .]

All cases employed 510 generations of 1000 neutrons, with a minimum of the first 10 generations discarded. Thus, each Monte Carlo result was based on $\sim 500,000$ neutron histories. This resulted in a maximum Monte Carlo standard deviation (σ) for any case of 0.0014.

Figure A.1 provides a sample SCALE 4.4a input, to determine k_{∞} for a mixture of $^{237}\text{NpO}_2\text{-H}_2\text{O}$ with an H: ^{237}Np atom ratio of 1.0.

Fig. A.1. Sample SCALE 4.4a Input
 (Case npo2hx10, to obtain k_{∞} for a $^{237}\text{NpO}_2\text{-H}_2\text{O}$ Mixture with $\text{H:}^{237}\text{Np} = 1.0$)

```
=csas25   parm=size=900000
case npo2hx10 - infinite system of 237npo2 mixed w/ h2o to give h/237np=1
238groupndf5 infhommedium
'237np (at density same as in theoretical-density oxide)
'237np density = 9.817 g/cc
np-237  1  0  2.4942-2  295 end
o       1  0  4.9884-2  295 end
h       1  0  2.4942-2  295 end
o       1  0  1.2471-2  295 end
end comp
more data dab=2000 end
case npo2hx10 - infinite system of 237npo2 mixed w/ h2o to give h/237np=1
read param
gen=510 npg=1000 nsk=10 nb8=2000 tba=5 tme=360
pki=yes xsl=yes pld=yes far=yes
end param
read geom
global
unit 1
cuboid  1  1  6p50.0
end geom
read bounds
xfc=mirror
yfc=mirror
zfc=mirror
end bounds
read mixt
sct=3 eps=0.1
end mixt
end data
end
```

A.4 MCNP 4c2 NCS Model

The NCS physics models and run parameters for MCNP 4c2 were analogous to the KENO NCS models, although the means of input differed as appropriate to the code input requirements.

Fig. A.2 provide a sample MCNP 4c2 input, to determine k_{∞} for a mixture of $^{237}\text{NpO}_2\text{-H}_2\text{O}$ with an $\text{H:}^{237}\text{Np}$ atom ratio of 1.0.

Fig. A.2. Sample MCNP 4c2 Input
 (Case npo210, to obtain k_{∞} for a $^{237}\text{NpO}_2\text{-H}_2\text{O}$ Mixture with $\text{H:}^{237}\text{Np} = 1.0$)

```
case npo210 - infinite system of 237npo2 mixed w/ h2o to give h/237np=1
C cell cards
1      1      1.12239E-01  -1      $NpO2 cube
2      0      0      1      $everything else

C Surface
*1     box  -50 -50 -50  100 0 0  0 100 0  0 0 100

C data card
mode n
imp:n 1 0
kcode  1000  1.0 10 510
ksrc   0. 0. 0.
C      NpO2  & H2O
ml     93237.50c  2.4942E-02
      8016.60c   6.2355E-02
      1001.50c   2.4942E-02
```

A.5 Results and Conclusions

Table A.1 provides the resulting infinite-system neutron multiplication factors. The value of "EALF" is the neutron energy (in MeV) corresponding to the average neutron lethargy of neutrons causing fission, as output by KENO-V.a.

Table A.1. Computed Infinite-System Neutron Multiplication Factors (k_{∞}) for $^{237}\text{Np-H}_2\text{O}$ or $^{237}\text{NpO}_2\text{-H}_2\text{O}$ Homogeneous Mixtures

H: ^{237}Np Atom Ratio	KENO V.a Results				MCNP 4c2 Results	
	k_{∞} for $^{237}\text{Np-H}_2\text{O}$	EALF (MeV)	k_{∞} for $^{237}\text{NpO}_2\text{-H}_2\text{O}$	EALF (MeV)	k_{∞} for $^{237}\text{Np-H}_2\text{O}$	k_{∞} for $^{237}\text{NpO}_2\text{-H}_2\text{O}$
0.0	1.62	1.40	1.34	1.41	1.61	1.33
0.5	1.15	1.55	1.02	1.52	1.15	1.02
1.0	0.92	1.61	0.84	1.58	0.92	0.84
1.5	0.78	1.64	0.71	1.61	0.78	0.71
2.0	0.67	1.66	0.62	1.63	0.67	0.62

Table A.1 computed results are consistent with ANS-8.15 prediction that uniform mixture of even a small quantity of hydrogen will reduce k_{∞} of those actinides that exhibit fission thresholds.

The KENO-V.a and MCNP 4c2 results compare very well. For each modeled material mixture, the corresponding KENO-V.a and MCNP 4c2 results differ by $\Delta k_{\text{eff}} \sim 0.01$ or less.

Table A.1 also indicates that presence of oxygen (e.g., due to the neptunium being in oxide form) reduces the criticality potential of ^{237}Np . Although the moderation effect of oxygen is slight, even just a few collisions of a fission neutron with oxygen will likely reduce the neutron energy to below the fission threshold of ^{237}Np . A similar effect would be anticipated due to presence of carbon. The DOT 9975 container construction incorporates Celotex, resulting in significant amounts of hydrogen, oxygen, and carbon as intervening materials between the individually small (relative to single-unit critical requirements) $^{237}\text{NpO}_2$ payloads. (Neutronic effects of the intervening Celotex are investigated in more detail in Appendix C.)

APPENDIX B

SCOPING COMPUTATIONS BASED ON ANSI/ANS-8.15 DATA

APPENDIX B. SCOPING COMPUTATIONS BASED ON ANSI/ANS-8.15 DATA

B.1 Introduction

This appendix provides NCS calculations that simulate selected (a) ANSI/ANS-8.15 critical estimates for ^{237}Np systems, (b) ANSI/ANS-8.15 subcritical limits, and (c) critical estimates for $^{237}\text{NpO}_2$ at oxide densities that are less than theoretical density.

These computations are considered to be "scoping" calculations since ^{237}Np critical experiment data is not available to quantitatively validate the computational results. These scoping calculations are used to compare the current computational methods to those employed as a basis for ANSI/ANS-8.15, and to support prior conclusions (in the body of this report) regarding the criticality physics of $^{237}\text{NpO}_2$ under conditions of reduced material density.

B.2 Computational Methods

The computational methods employed for Appendix B calculations are the same as described in Appendix A, Section A.2.

For some SCALE 4.4a computations of this appendix, the CSAS4 control sequence was employed. The CSAS4 sequence iteratively invokes the CSAS25 modules as a search routine. Where CSAS4 was employed, the system dimensions were varied to determine a computed value of k_{eff} that was within 0.001 of unity (i.e., in absence of a supporting validation, a computed value of $k_{\text{eff}} = 1.00$ is assumed to represent a critical system). For CSAS4 runs, the geometry model of the final CSAS25 iteration was accepted as the result.

B.3 SCALE 4.4a NCS Models

The NCS geometry model for all cases of this appendix consisted of a simple sphere of either ^{237}Np or $^{237}\text{NpO}_2$. For reflected cases, a 20-cm thick close-fitting spherical SS304L steel reflector was modeled.

For material models, isotopic weights and Avogadro's number were obtained from Reference 14. The theoretical density of ^{237}Np metal was modeled as 20.476 g/cm^3 , resulting in an input atom density specification of $N_{237\text{Np}} = 5.2019 \times 10^{-2} \text{ a/bn-cm}$. The theoretical density of $^{237}\text{NpO}_2$ was modeled as 11.143 g/cm^3 , obtained with input atom density specifications of $N_{237\text{Np}} = 2.4942 \times 10^{-2} \text{ a/bn-cm}$ and $N_{\text{O}} = 4.9884 \times 10^{-2} \text{ a/bn-cm}$. For consideration of $^{237}\text{NpO}_2$ at lesser densities, the dimensionless fractional density ($\rho/\rho_{\text{theoretical}}$) was applied to the theoretical-density $^{237}\text{NpO}_2$ atom density specifications.

To model the stainless steel reflector, the material model described by Westfall⁷ was employed*. The input atom density specifications for SS304L were $N_{\text{Fe}} = 5.9358 \times 10^{-2}$ a/bn-cm, $N_{\text{Cr}} = 1.7428 \times 10^{-2}$ a/bn-cm, $N_{\text{Ni}} = 7.7199 \times 10^{-2}$ a/bn-cm, and $N_{\text{Mn}} = 1.7363 \times 10^{-3}$ a/bn-cm.

All cases employed 510 generations of 1000 neutrons, with a minimum of the first 10 generations discarded. Thus, each Monte Carlo result was based on ~ 500,000 neutron histories. This resulted in a maximum Monte Carlo standard deviation (σ) for any case of 0.0015.

Figure B.1 provide a sample SCALE 4.4a input, to determine the radius corresponding to $k_{\text{eff}} = 1.000$ for theoretical-density $^{237}\text{NpO}_2$ with a 20-cm thick SS304L reflector.

Fig. B.1. Sample SCALE 4.4a Input
(Case npst04, to obtain the radius of theoretical-density $^{237}\text{NpO}_2$ corresponding to $k_{\text{eff}} = 1.000$, with spherical geometry and a 20-cm thick SS304L reflector)

```
#csas4      parm=(size=2500000)
case npst04 - find critical radius of ss-reflected sphere of 237npo2
238groupndf5 infhommedium
'material 1 - 237npo2 @ 11.143 g/cc
np-237      1 0 2.4942e-02 end
o           1 0 4.9883e-02 end
'material 2 - westfall nucsci&eng model, ss304l @ 7.92 g/cc
'69.5 w/o fe, 19 w/o cr, 9.5 w/o ni, and 2 w/o mn
fe          2 0 5.9358e-02 end
cr          2 0 1.7428e-02 end
ni          2 0 7.7199e-03 end
mn          2 0 1.7363e-03 end
end comp
more data dab=2000 end
case npst04 - find critical radius of ss-reflected sphere of 237npo2
read param
gen=510 npg=1000 nsk=10
nb8=2000 tba=5 tme=240
end param
read geom
sphere      1 1 12.0
replicate  2 1 20.0 1
end geom
read mixt
sct=3 eps=0.1
end mixt
end data
read search
critical dimension
kef=1.000
eps=0.001
pas=15
more
alter      unit=1 reg=1 r=1.0
maintain unit=1 reg=2 all=1.0
-con=-0.0
+con=+0.5
end search
end
```

* A typographical error is assumed to be present in the Reference 7 description of stainless steel. The steel model is described as SS304L with a density of 7.92 g/cm^3 , with weight fractions of 0.695 for iron, 0.19 for nickel, 0.095 for chromium, and 0.02 for manganese. However, typical stainless steels contain a chromium content exceeding that of the nickel content. For typical SS304-series stainless steels, the chromium content is approximately twice that of nickel. The intended Reference 7 description of SS304L is assumed to be as described above, except that the weight fraction of chromium is assumed to be 0.19 and the weight fraction of nickel is assumed to be 0.095.

B.4 MCNP 4c2 NCS Model

The NCS physics models for MCNP 4c2 were similar to the SCALE 4.4a NCS models, although the means of input differed as appropriate to the code input requirements. For CSAS4 runs, the final converged SCALE geometric result was used as the geometry specification for the analogous MCNP 4c2 run.

Figure B.2 provide a sample MCNP 4c2 input, to determine k_{eff} for a SS304L-reflected sphere of theoretical-density $^{237}\text{NpO}_2$. The fissionable material radius employed for this MCNP 4c2 case is the result of SCALE 4.4a case npst04 (result from the SCALE 4.4 a input shown on Fig. B.1, above).

Fig. B.2. Sample MCNP 4c2 Input
(Case to obtain k_{eff} for a SS304L-reflected theoretical-density $^{237}\text{NpO}_2$ sphere of radius 17.385 cm)

```
case npst04 - critical ss-reflected sphere of 237npO2
C cell cards
1      1      7.4826E-02  -1                $NpO2 sphere
2      2      8.6242E-02   1 -2          $$$SS reflector
3      0                2                $everything else

C Surface
1      so  17.385
2      so  37.385

C data card
mode n
imp:n 1 1 0
kcode  1000  1.0 10 510
sdef   pos=0 0 0  rad=d1
sil    0 17.38
spl    -21  2
C      NpO2
m1     93237.50c 1
        8016.50c 2
C      SS
m2     26000.50c 5.9358E-02
        24000.50c 1.7428E-02
        28000.50c 7.7199E-03
        25055.50c 1.7363E-03
```

B.5 Results and Conclusions

Table B.1 provides the results of calculations modeling the two ANSI/ANS-8.15 subcritical limits: 20 kg of ^{237}Np metal for steel-reflected conditions, and 90 kg of ^{237}Np as oxide, also for steel-reflected conditions. The value of "EALF" is the neutron energy (in MeV) corresponding to the average neutron lethargy of neutrons causing fission, as output by KENO-V.a.

**Table B.1. Computed SCALE 4.4a and MCNP 4c2 Results
Simulating ANSI/ANS-8.15-Steel-Reflected ^{237}Np Subcritical Limits**

SCALE Case Name	SCALE 4.4a Results			MCNP 4c2 Results		Considered ANSI/ANS-8.15 Subcritical Limit
	k_{eff}	σ	EALF (MeV)	k_{eff}	σ	
npst05	0.8647	0.0012	1.52	0.8632	0.0009	20 kg ^{237}Np metal limit
npst06	0.8782	0.0010	1.44	0.8718	0.0009	90 kg ^{237}Np limit as oxide

To investigate the moderating influence of oxygen present in the oxide form, a variation of SCALE case npst06 was executed. Case npst06a had the same NCS model as case npst06, except that the input atom density for oxygen was eliminated. For case npst06a, $k_{\text{eff}} = 0.9206$ with $\sigma = 0.0012$ and EALF = 1.46 MeV. (The corresponding MCNP 4c2 result was $k_{\text{eff}} = 0.9170$ with $\sigma = 0.0010$.)

Table B.1 results are consistent with the expectation that the neutron multiplication factor (k_{eff}) values for the ANSI/ANS-8.15 ^{237}Np subcritical limits should be much less than unity. The result of case npst06a indicates that the neutronic effect of oxygen is to reduce k_{eff} (increase critical mass requirements) for ^{237}Np , an indication that is consistent with Appendix A k_{∞} results.

Table B.2 provides results for SCALE 4.4a search calculations used to derive spherical critical mass estimates for ^{237}Np metal and $^{237}\text{NpO}_2$ at theoretical density, for conditions of no reflector and for a 20-cm thick steel (SS304L) reflector. For each SCALE 4.4a-derived result, the MCNP 4c2-computed k_{eff} value is reported. The result of these calculations are meant for comparison to similar estimates reported in Appendix B of ANSI/ANS-8.15.

Each ^{237}Np metal mass estimate of Table B.2 is within the range of corresponding critical estimates provided in Appendix A of ANSI/ANS-8.15. For $^{237}\text{NpO}_2$, each mass estimate of Table B.4 is about 16% greater than the corresponding ANSI/ANS-8.15 estimate.

**Table B.2. Computed SCALE 4.4a and MCNP 4c2 Results
Simulating ANSI/ANS-8.15 ²³⁷Np Appendix A Critical Estimates**

SCALE Case Name	<u>SCALE 4.4a Results</u>			<u>MCNP 4c2 Results</u>		<u>Considered ANSI/ANS- 8.15 Critical Estimate</u>
	radius (cm)	EALF (MeV)	Mass of ²³⁷ Np for k _{eff} =1.0 (kg ²³⁷ Np)	(k _{eff})	(σ)	
npst01	9.2597	1.57	68.1	0.9998	0.0011	Bare sphere, ²³⁷ Np metal
npst02	7.8056	1.49	40.8	0.9977	0.0010	SS304L-reflected sphere of ²³⁷ Np metal
npst03	20.155	1.49	337	0.9961	0.0011	Bare sphere, ²³⁷ NpO ₂ at theoretical density
npst04	17.385	1.42	216	0.9922	0.0010	SS304L-reflected sphere, ²³⁷ NpO ₂ at theoretical density

Table B.3 provides results for SCALE 4.4a search calculations used to derive spherical critical mass estimates for ²³⁷NpO₂ at reduced density, for conditions of no reflector and for a 20-cm thick steel (SS304L) reflector. For each SCALE 4.4a-derived result, the MCNP 4c2-computed k_{eff} value is reported. For comparison, Table B.2 results for ²³⁷NpO₂ at theoretical density are included.

The core-density technique provides the relationship of the critical mass at a reduced density (M_c) to the critical mass at a reference density (M_{co}) as a function of the density reduction factor (ρ/ρ_o):

$$\frac{M_c}{M_{co}} = \left(\frac{\rho}{\rho_o} \right)^{-n}$$

The values of the core density exponent *n* may be estimated from table B.5 data, using ρ_o = ρ_{theoretical}:

$$n = - \frac{\ln(M_c / M_{co})}{\ln(\rho / \rho_o)}$$

For a bare sphere of ²³⁷NpO₂, comparison of results for cases npst09 and npst03 yield *n* = 2.01. Comparison of SCALE results for cases npst10 and npst03 yields *n* = 2.00. These predictions are consistent with theory: the value of *n* for an unreflected sphere of any type of fissionable material should be exactly 2.

For a SS304L-reflected sphere of ²³⁷NpO₂, comparison of results for cases npst07 and npst04 yield *n* = 1.85. Comparison of SCALE results for cases npst08 and npst04 yields *n* = 1.88. These predictions are consistent with the Section 3.5 conclusion that for a SS304L-reflected sphere of ²³⁷NpO₂, the core-density exponent should be within the range of *n* = 1.4 to 2.0.

Table B.3. Computed SCALE 4.4a and MCNP 4c2 Results of $^{237}\text{NpO}_2$ Critical Estimates as a Function of Density Reduction Factor ($\rho/\rho_{\text{theoretical}}$)

Case Name	SCALE 4.4a Results			MCNP 4c2 Results		Reflector and Density Reduction Factor
	radius (cm)	EALF (MeV)	Mass of ^{237}Np for $k_{\text{eff}}=1.0$ (kg ^{237}Np)	(k_{eff})	(σ)	
npst03	20.155	1.49	337	0.9961	0.0011	Bare sphere, $\rho/\rho_{\text{th}} = 1.0$
npst09	40.343	1.49	1350	0.9975	0.0010	Bare sphere, $\rho/\rho_{\text{th}} = 0.5$
npst10	201.07	1.48	33400	0.9958	0.0010	Bare sphere, $\rho/\rho_{\text{th}} = 0.1$
npst04	17.385	1.42	216	0.9922	0.0010	SS304L-reflected sphere, $\rho/\rho_{\text{th}} = 1.0$
npst07	33.403	1.41	776	0.9924	0.0010	SS304L-reflected sphere, $\rho/\rho_{\text{th}} = 0.5$
npst08	158.74	1.38	16500	0.9932	0.0010	SS304L-reflected sphere, $\rho/\rho_{\text{th}} = 0.1$

The KENO-V.a and MCNP 4c2 results compare very well. For each modeled configuration, the corresponding KENO-V.a and MCNP 4c2 results differ by $\Delta k_{\text{eff}} \sim 0.01$ or less.

APPENDIX C

SCOPING COMPUTATIONS FOR DOT 9975 SINGLE UNITS AND INFINITE ARRAYS

APPENDIX C. SCOPING COMPUTATIONS FOR DOT 9975 SINGLE UNITS AND INFINITE ARRAYS

C.1 Introduction

This appendix provides NCS calculations that estimate neutron multiplication factors (k_{eff}) for $^{237}\text{NpO}_2$ -loaded DOT 9975 containers.

These computations are considered to be "scoping" calculations since ^{237}Np critical experiment data is not available to quantitatively validate the computational results. The scoping calculations are used to qualitatively support conclusions of Sections 6.1 and 6.2 that the low density of the $^{237}\text{NpO}_2$ (as an array average) and the presence of neutron moderators (as part of the DOT 9975 container construction) preclude effective neutron interaction of the DOT 9975 container payloads.

C.2 Computational Method

The computational methods employed for Appendix C calculations are the same as described in Appendix A, Section A.2.

C.3 SCALE 4.4a NCS Model

The NCS model for the DOT 9975 container based on NCS model specifications given in the current DOT 9975 SARP¹⁰.

Most of the container material models were obtained from Tables 6.15 and 6.16 of the SARP. The intended density of the aluminum "honeycomb" axial impact absorbers is assumed to be 0.28 g/cm^3 , based on the sample SCALE inputs provided in the SARP.

The base geometry model is that shown by Fig. 6.13 of the DOT 9975 SARP. (For that figure, the legend does not correctly correlate with the graphic. The two low-density aluminum regions of the NCS model are (a) the annular section of Unit 3 and (b) the disk section of Unit 6. All other components of the SCV and PCV are stainless steel in the base container model.)

To simulate an infinite array of DOT 9975 containers, the cuboid region that tightly encloses the outermost cylindrical surface of the container model is specified with appropriate boundary conditions. These boundary conditions simulate an infinite three-dimensional lattice of containers. Along the z-axis (the axis along which stacked containers are simulated), the containers are all modeled as being upright by using the "periodic" boundary condition. Along the x- and y-axes, the "mirror" boundary condition was used.

All cases employed 510 generations of 1000 neutrons, with a minimum of the first 10 generations discarded. Thus, each Monte Carlo result was based on $\sim 500,000$ neutron histories. The Monte Carlo standard deviation (σ) for all cases were less than 0.001.

Figure C.1 shows sample scale input for Case C04.

Fig. C.1. Sample SCALE 4.4a Input

(Case c04. Models an infinite array of DOT 9975 containers, each loaded with 6 kg ²³⁷Np as oxide, oxide at half theoretical density, oxide in a cylindrical shape with a height-to-diameter ratio of unity)

```
=csas25      parm=size=1000000
case c04 - 9975 w/ 1/2 den cyl unreflected
238groupndf5 infhommedium
'material 1 - 237npo2 @ 0.5 x 11.143 g/cc
np-237      1 0 1.2471e-02 end
o          1 0 2.4942e-02 end
'material 2 - celotex: c6h10o5 @ 0.20 g/cc
c          2 0 4.4569e-03 end
h          2 0 7.4282e-03 end
o          2 0 3.7141e-03 end
'material 3 - ss304 @ 7.9 g/cc
fe         3 0 6.0360e-02 end
mn         3 0 1.7321e-02 end
cr         3 0 1.6471e-02 end
si         3 0 1.6940e-03 end
c          3 0 3.1696e-04 end
ni         3 0 6.4834e-03 end
'material 4 - aluminum @ 2.7 g/cc
al         4 0 6.0262e-02 end
'material 5 - aluminum honeycomb @ 0.28 g/cc
al         5 0 6.2494e-03 end
'material 6 - water @ 0.9982 g/cc
h          6 0 6.6737e-02 end
o          6 0 3.3369e-02 end
'material 7 - lead @ 11.29 g/cc
pb         7 0 3.2813e-02 end
end comp
more data dab=2000 end
case c04 - 9975 w/ 1/2 den cyl unreflected
read param
gen=510 npg=1000 nsk=10 nub=yes nb8=2000 tba=5 tme=360
end param
read geom
unit 1
com='payload elevation of 9975'
com=' w/ 6 kg np as 1/2 th dens npo2 cyl'
cylinder  1 1  5.79425 29.7015 18.113
cylinder  0 1  6.571 59.12 18.113
cylinder  3 1  7.144 59.12 17.539
cylinder  0 1  7.702 59.12 17.539
cylinder  3 1  8.414 59.12 17.539
cylinder  0 1  9.525 59.12 17.539
cylinder  7 1 10.795 59.12 17.539
cylinder  2 1 21.415 59.12 17.539
cylinder  3 1 21.536 59.12 17.539
cuboid    0 1 4p21.536 59.12 17.539
unit 2
com='top of primary containment - ss304 pcv lid'
cylinder  3 1  7.455 62.61 59.12
cylinder  0 1  7.702 62.61 59.12
cylinder  3 1  8.414 62.61 59.12
cylinder  0 1  9.525 62.61 59.12
cylinder  7 1 10.795 62.61 59.12
cylinder  2 1 21.415 62.61 59.12
cylinder  3 1 21.536 62.61 59.12
cuboid    0 1 4p21.536 62.61 59.12
```

Fig. C.1. Sample SCALE 4.4a Input (Continued)

```
unit 3
com='primary containment ss304 nut and al honeycomb'
cylinder 3 1 3.175 63.90 62.61
cylinder 0 1 4.763 67.06 62.61
cylinder 5 1 7.702 67.06 62.61
cylinder 0 1 7.702 68.49 62.61
cylinder 3 1 8.414 68.49 62.61
cylinder 0 1 9.525 68.49 62.61
cylinder 7 1 10.795 68.49 62.61
cylinder 2 1 21.415 68.49 62.61
cylinder 3 1 21.536 68.49 62.61
cuboid 0 1 4p21.536 68.49 62.61
unit 4
com='top of secondary containment - ss304 scv lid'
cylinder 3 1 9.042 71.98 68.49
cylinder 0 1 9.525 71.98 68.49
cylinder 7 1 10.795 71.98 68.49
cylinder 2 1 21.415 71.98 68.49
cylinder 3 1 21.536 71.98 68.49
cuboid 0 1 4p21.536 71.98 68.49
unit 5
com='al shield top'
cylinder 0 1 9.525 73.27 71.98
cylinder 7 1 10.795 73.27 71.98
cylinder 4 1 10.795 74.54 71.98
cylinder 2 1 21.415 74.54 71.98
cylinder 3 1 21.536 74.54 71.98
cuboid 0 1 4p21.536 74.54 71.98
unit 6
com='pcv legs, al honeycomb and scv bottom'
cylinder 0 1 5.113 17.539 16.575
cylinder 3 1 5.715 17.539 16.575
cylinder 0 1 7.702 17.539 16.575
cylinder 5 1 7.702 17.539 14.034
cylinder 3 1 8.414 17.539 13.412
cylinder 0 1 9.525 17.539 13.412
cylinder 7 1 10.795 17.539 13.412
cylinder 2 1 21.415 17.539 13.412
cylinder 3 1 21.536 17.539 13.412
cuboid 0 1 4p21.536 17.539 13.412
unit 7
com='scv legs and bottom of lead shield'
cylinder 0 1 6.410 13.412 12.447
cylinder 3 1 7.065 13.412 12.447
cylinder 0 1 9.525 13.412 12.447
cylinder 7 1 10.795 13.412 11.177
cylinder 2 1 21.415 13.412 11.177
cylinder 3 1 21.536 13.412 11.177
cuboid 0 1 4p21.536 13.412 11.177
unit 8
com='al top plate and celotex plus void plus drum'
cylinder 4 1 14.224 75.81 74.54
cylinder 2 1 21.415 84.70 74.54
cylinder 0 1 21.415 85.847 74.54
cylinder 3 1 21.536 85.968 74.54
cuboid 0 1 4p21.536 85.968 74.54
unit 9
com='al bottom plate and celotex plus void plus drum'
cylinder 4 1 14.224 11.177 9.907
cylinder 2 1 21.415 11.177 1.271
cylinder 0 1 21.415 11.177 0.121
cylinder 3 1 21.536 11.177 0.000
cuboid 0 1 4p21.536 11.177 0.000
```

Fig. C.1. Sample SCALE 4.4a Input (Continued)

```
global
unit 10
array 1 -21.536 -21.536 0.0
replicate 0 1 6r30 1
end geom
read array
ara=1 nux=1 nuy=1 nuz=9 fill 9 7 6 1 2 3 4 5 8 end fill
end array
read mixt
sct=3 eps=0.1
end mixt
read plot
pic=mat
clr= 0 255 255 255
      1 255 255 0
      2 255 120 0
      3 180 180 180
      4 240 240 240
      5 0 255 0
      6 255 0 255
      7 255 0 255 end color
ttl=/plan view through model at payload elevation/
lpi=10
nax=640
xul=-55.0 yul= 55.0 zul=23.3775
xlr= 55.0 ylr=-55.0 zlr=23.3775
uax=1.0 vdn=-1.0 end
ttl=/plan view through 9975 at payload elevation/
lpi=10
nax=640
xul=-21.6 yul= 21.6 zul=23.3775
xlr= 21.6 ylr=-21.6 zlr=23.3775
uax=1.0 vdn=-1.0 end
ttl=/plan view through lead & scv at payload elevation/
lpi=10
nax=640
xul=-11.0 yul= 11.0 zul=23.3775
xlr= 11.0 ylr=-11.0 zlr=23.3775
uax=1.0 vdn=-1.0 end
ttl=/sect view through model looking in +y direction/
lpi=10
nax=640
xul=-53.0 yul= 0.00 zul=120.0
xlr= 53.0 ylr= 0.00 zlr=-35.0
uax=1.0 wdn=-1.0 end
ttl=/sect view through 9975 looking in +y direction/
lpi=10
nax=640
xul=-23.0 yul= 0.00 zul=87.0
xlr= 23.0 ylr= 0.00 zlr=-1.0
uax=1.0 wdn=-1.0 end
ttl=/sect view through lead & scv looking in +y direction/
lpi=10
nax=640
xul=-12.0 yul= 0.00 zul=76.0
xlr= 12.0 ylr= 0.00 zlr= 9.0
uax=1.0 wdn=-1.0 end
end plot
end data
end
```

C.4 Results and Conclusions

Table C.1 provides the results of SCALE 4.4a calculations (CSAS25 routine) that consider DOT 9975 payloads of $^{237}\text{NpO}_2$ at theoretical density. The considered payload geometries are a sphere of input radius 5.26442 cm, or a cylinder having a height-to-diameter ratio of unity (radius = 4.599 cm; height = 9.1978 cm)

The results of Table C.1 support these observations:

- (1) The DOT 9975 container causes a negligible increment to the k_{eff} of the payload, due to provision of an enclosing, neutron-reflecting environment.
- (2) Reflector conditions external to the DOT 9975 container have a negligible worth to the container payload k_{eff} .
- (3) There is near-negligible (productive) neutron interaction between the DOT 9975 container payloads.
- (4) A range of potential shielding material additions (steel or lead) was considered that bounded the maximum range of variation (based on the current SARP designs for the PCV, SCV, and lead liner).

As a result of these factors, the computed k_{eff} for an individual, unreflected container payload differs little from computed k_{eff} values for individual loaded containers or even for infinite container arrays.

Table C.2 provides similar results as Table C.1, for cases modeling an oxide density at half of theoretical density. The payload is modeled as a cylinder with a height-to-diameter ratio of unity (radius = 5.79425 cm, height = 11.5885 cm). Table C.3 cases model a fissionable material density of 25% of theoretical oxide density. The results for Tables C.2 and C.3 support the four observations noted above.

**Table C.1. Computed SCALE 4.4a Results:
Single-Units and Infinite Arrays of DOT 9975 Containers,
Oxide Payload Modeled as Single-Unit, Theoretical-Density Oxide Unit**

Case Name	Modeled Configuration	k_{eff}
up01	Unreflected sphere of theoretical-density oxide (no container - simulates payload before placement into the DOT 9975 container) Mass = 6 kg ^{237}Np , sphere radius = 5.264 cm, material density = 11.143 g oxide/cm ³	0.396
c01	6 kg ^{237}Np sphere in single, unreflected DOT 9975 container	0.411
c02	6 kg ^{237}Np sphere in single, water-reflected DOT 9975 container	0.413
c03	6 kg ^{237}Np sphere in single, concrete-reflected DOT 9975 container	0.415
c10	Infinite array of DOT 9975 containers, each loaded with a theoretical-density, 6 kg ^{237}Np sphere	0.424
c13	Infinite array of DOT 9975 containers, each loaded with a 6 kg ^{237}Np theoretical-density oxide cylinder having a height-to-diameter ratio of unity	0.416
c14	Same as c13, change void regions inside the lead liner but outside the SCV with lead	0.421
c16	Same as c14, also replace void regions and low-density aluminum regions inside the SCV but outside the PCV with lead	0.426
c18	Same infinite array as c16, change boundary conditions on z-faces from "periodic" to "mirror"; results in reduced minimum axial separation of payloads within the array.	0.429
c19	Same as c16, also replace void regions within the PCV with lead	0.453
c23	Same as c19, single unreflected DOT 9975 container	0.445
c15	Same as c13, change void regions inside the lead liner but outside the SCV with SS304L	0.420
c17	Same as c15, also replace void regions and low-density aluminum regions inside the SCV but outside the PCV with SS304L	0.428
c20	Same as c17, also replace void regions within the PCV with SS304L	0.461
c24	Single unreflected DOT 9975 container, same container model as c20	0.457
c26	Same infinite array as c10, reduce celotex material density to 1/10 of original value to model fire-induced Celotex loss	0.461
c27	Same infinite array as c10, increase the payload to 12 kg ^{237}Np as a theoretical-density oxide sphere.	0.491

- Two additional observations (based on collective data of Tables C.1, C.2, and C.3) are that
- (5) The DOT 9975 individual container k_{eff} (essentially equal to the array k_{eff}) is primarily determined by the considered density of the oxide payload. The k_{eff} value is maximized when the density is maximized, as predicted by core-density correlation.
 - (6) Even with the most reactive, optimized models considered for potential DOT 9975 payloads and shielding configurations, no single container or array k_{eff} result was found exceeding a value of 0.5.

**Table C.2. Computed SCALE 4.4a Results:
Single-Units and Infinite Arrays of DOT 9975 Containers,
6 kg ²³⁷Np as Half-Theoretical-Density Oxide Per Container.**

Case Name	Modeled Configuration	k _{eff}
up04	Unreflected cylinder of half-theoretical-density oxide (no container - simulates payload before placement into the DOT 9975 container) Cylinder radius = 5.79425 cm, height = 11.5885 cm, and material density =5.5715 g oxide/cm ³	0.251
c04	Cylinder in single, unreflected DOT 9975 container	0.277
c05	Cylinder in single, water-reflected DOT 9975 container	0.276
c06	Cylinder in single, concrete-reflected DOT 9975 container	0.278
c11	Infinite array of DOT 9975 containers, each loaded with a half-theoretical-density cylinder	0.292
c21	Same as c11, change all void regions and all low-density aluminum regions within the lead liner to SS304L	0.322

**Table C.3. Computed SCALE 4.4a Results:
Single-Units and Infinite Arrays of DOT 9975 Containers,
6 kg ²³⁷Np as Quarter-Theoretical-Density Oxide Per Container.**

Case Name	Modeled Configuration	k _{eff}
up07	Unreflected cylinder of quarter-theoretical-density oxide (no container - simulates payload before placement into the DOT 9975 container) Cylinder radius = 6.571 cm, height = 18.0214 cm, and material density =2.79 g oxide/cm ³	0.158
c07	Cylinder in single, unreflected DOT 9975 container	0.185
c08	Cylinder in single, water-reflected DOT 9975 container	0.185
c09	Cylinder in single, concrete-reflected DOT 9975 container	0.186
c12	Infinite array of DOT 9975 containers, each loaded with a quarter-theoretical-density cylinder	0.202
c22	Same as c12, change all void regions and all low-density aluminum regions within the lead liner to SS304L	0.218

APPENDIX D

**COMPUTATIONS OF CRITICAL EXPERIMENTS INVOLVING
HEU METAL CYLINDERS IN ARRAYS**

APPENDIX D. COMPUTATIONS OF CRITICAL EXPERIMENTS INVOLVING HEU METAL CYLINDERS IN ARRAYS

D.1 Introduction

This appendix provides NCS calculations of critical experiments reported by D. W. Magnuson in Y-DR-83¹¹ and Y-DR-109¹². The purpose of these early 1970s experiments was to provide data for design and development of radioactive materials shipping containers. The experiments included variations where Celotex, plywood, or plastic was interspersed among a 2 x 2 x 2 array of eight large [~ 21 kg U(93.2) each] HEU metal cylinders. Experiments were also performed with no intervening moderator materials. Two reflector conditions were examined: a concrete reflector or a polyethylene reflector about all six sides of each array.

These experiments are pertinent. Because the computational method of this appendix (SCALE 4.4a CSAS25 routine with ENDF/B-V data) can be successfully applied, there is better confidence that high-energy fission neutron transport through and energy loss within Celotex are properly simulated (calculations of Appendices C and E).

Also, the experimental units are comparable in form and k_{eff} to the HEU metal units considered in the mixed DOT 9975/HEU arrays (calculations of Appendix D). This lends confidence that the source neutron spectrum of the near-critical HEU units and the migration of those neutrons into the DOT 9975 insulation materials is reasonably simulated by the computational method.

The purpose of these critical experiment calculations is qualitative; no upper safety limit will be derived.

D.2 Computational Method

The computational methods employed for Appendix D calculations are the same as described in Appendix A, Section A.2. Only the SCALE 4.4a CSAS25 method was used; this is the same method applied for Appendix C and E calculations.

D.3 SELECTED EXPERIMENTS

Only about half of the fissionable material configurations of Y-DR-83 and Y-DR-109 were used. Reported configurations were omitted on the following bases:

- boron was present as a neutron-absorbing material between units (strong thermal neutron absorbers are not relevant to the considered $^{237}\text{NpO}_2$ processes),
- no value of the experimental k_{eff} was reported (may represent a planned experiment rather than one that was performed),
- the reported experimental k_{eff} differed from unity by more than β , the delayed neutron fraction for ^{235}U (~ 0.007) (these configurations potentially represent significant extrapolations from actual experimental observations).

Using the above criteria, the selected experimental configurations were Y-DR-83 experiment numbers 1 through 3, and Y-DR-109 experiment numbers 1, 3, 5, 6, 7, 11, 12, and 18 through 21.

Table D.1 summarizes conditions of these 14 experiments.

Table D.1. Selected Y-DR-83 and Y-DR-109 Experiments

Reference	Expt. #	Case Name	Array Reflector	Intervening Materials
Y-DR-83	1	ydr83a	Polyethylene	Plywood (cellulose at 0.53 g/cm^3)
Y-DR-83	2	ydr83b	Polyethylene	Celotex (cellulose at 0.215 g/cm^3)
Y-DR-83	3	ydr83c	Polyethylene	Celotex plus layer of Plexiglas
Y-DR-109	1	ydr109a	Concrete	Void
Y-DR-109	3	ydr109c	Concrete	Void
Y-DR-109	5	ydr109e	Concrete	Void
Y-DR-109	6	ydr109f	Concrete	Void
Y-DR-109	7	ydr109g	Concrete	Void
Y-DR-109	11	ydr109k	Concrete	Void
Y-DR-109	12	ydr109l	Concrete	Void
Y-DR-109	18	ydr109r	Polyethylene	Vermiculite (0.34 g/cm^3)
Y-DR-109	19	ydr109s	Polyethylene	Vermiculite
Y-DR-109	20	ydr109t	Polyethylene	Vermiculite
Y-DR-109	21	ydr109u	Polyethylene	Vermiculite

D.4 SCALE 4.4a NCS Models

The NCS geometry models for the Y-DR-83 and Y-DR-109 experiments are based on the KENO-type input specifications provided by Magnuson in each of the reports. Magnuson also provides the atomic density models for various experimental materials. These were used without change except that in Y-DR-83, there is a typographical error in the atom density specification for the full-density polyethylene model. The stated hydrogen atom density of $7.90 \times 10^{-3} \text{ a/bn-cm}$ should be $7.90 \times 10^{-2} \text{ a/bn-cm}$.

All cases employed 525 generations of 2000 neutrons, with a minimum of the first 25 generations discarded. Thus, each Monte Carlo result was based on $\sim 1,000,000$ neutron histories. The Monte Carlo standard deviation (σ) for all cases was ~ 0.0008 .

Fig. D.1. Sample SCALE 4.4a Input

(Input file ydr83a - Critical experiment with 2 x 2 x 2 arrays of ~ 21 kg U(93.2) cylinders, each cylinder enclosed in cutout in a split cube of plywood)

```
=csas25          parm=size=2000000
y-dr-83 case 1
238gr inf
'fuel
u-235  1  0.0 4.448e-2 end
u-238  1  0.0 3.201e-3 end
'wood
c      2  0.0 1.182e-2 end
h      2  0.0 1.970e-2 end
o      2  0.0 9.850e-3 end
'polyethylene
c      3  0.0 3.95e-2  end
h      3  0.0 7.90e-2  end
end comp
y-dr-83 case 1
read para gen=525 npg=2000 nsk=25 fdn=yes nub=yes end para
read geom
unit 1
cylinder 1 1 5.76 2p5.4
cuboid  2 1 4p12.08 2p13.82
cuboid  0 1 2p14.07 2p12.8 2p13.82
global
unit 100
array 1 0 0 0
replicate 3 1 6r20 1
end geom
read array
ara=1 nux=2 nuy=2 nuz=2 fill f1 end fill
end array
read mixt
sct=3 eps=0.1
end mixt
end data
end
```

D.5 Results and Conclusions

Table D.2 provides the results of SCALE 4.4a calculations (CSAS25 routine) for the selected critical or near-critical configurations.

The results of Table D.2 indicate the computational method can reasonably model the neutronic behavior of the critical experiments.

Two experiments are of particular interest: experiments 1 and 2 of Y-DR-83. The first experiment (modeled as case ydr83a) uses wood as the material between the HEU units. The second experiment (case ydr83b) uses Celotex. The Celotex material model is nearly identical to that described in the DOT 9975 SARP differing slightly only in overall material density. Like the Celotex, the wood is modeled as cellulose, at a density ~ 2.65 times that of the Celotex model for the DOT 9975. The significant computed Δk_{eff} results for the perturbed cases indicates that the experiment configurations are sensitive to presence of these intervening low-density moderators. The good agreement of the computational results with the experimental results support that neutron transport in the cellulosic materials is reasonably simulated by the computational technique.

**Table D.2. SCALE 4.4a Results:
Selected Y-DR-83 and Y-DR-109 Critical Experiments**

Reference	Expt. #	Case Name	Configuration k_{eff}	Computed k_{eff}	σ	EALF (MeV)
Y-DR-83	1	ydr83a	1.0005	1.0006	0.0009	0.011
Y-DR-83	2	ydr83b	0.9979	0.9976	0.0009	0.012
Y-DR-83	3	ydr83c	0.9950	0.9993	0.0010	0.011
Y-DR-109	1	ydr109a	1.0002	1.0093	0.0008	0.059
Y-DR-109	3	ydr109c	1.0005	1.0084	0.0008	0.058
Y-DR-109	5	ydr109e	1.0060	1.0133	0.0008	0.057
Y-DR-109	6	ydr109f	0.9962	1.0039	0.0008	0.056
Y-DR-109	7	ydr109g	1.0057	1.0149	0.0009	0.052
Y-DR-109	11	ydr109k	1.0017	1.0105	0.0008	0.056
Y-DR-109	12	ydr109l	0.9968	1.0014	0.0008	0.067
Y-DR-109	18	ydr109r	1.0005	1.0128	0.0008	0.018
Y-DR-109	19	ydr109s	1.0007	1.0123	0.0007	0.017
Y-DR-109	20	ydr109t	1.0016	1.0108	0.0009	0.016
Y-DR-109	20	ydr109u	1.0013	1.0112	0.0008	0.017
Perturbed Cases (Wood or Celotex omitted)						
Y-DR-83	1	ydr83ax	n/a	0.9484	0.0008	0.012
Y-DR-83	2	ydr83bx	n/a	0.9701	0.0008	0.011

APPENDIX E

**SCOPING COMPUTATIONS FOR ADJACENT ARRAYS OF
DOT 9975 CONTAINERS AND HEU UNITS**

APPENDIX E. SCOPING COMPUTATIONS FOR ADJACENT ARRAYS OF DOT 9975 CONTAINERS AND HEU UNITS

E.1 Introduction

This appendix provides scoping NCS calculations to characterize the neutron interaction potential between the DOT 9975 $^{237}\text{NpO}_2$ payloads and nearby fissionable material items.

These computational results cannot be validated due to lack of ^{237}Np experimental data. However, the results are consistent with expected system behavior.

Within an array of DOT 9975 containers, effective neutron interaction is lacking because of the low-density scattering and moderating materials (Celotex) between the payloads, the small volume fraction of the array that is occupied by the payloads, and the nuclear characteristic that ^{237}Np is nonfissile and exhibits a fission threshold.

These same factors serve to inhibit effective neutron interaction between contents of the DOT 9975 containers and exterior fissionable material items.

E.2 Computational Method

The computational methods employed for Appendix E calculations are the same as described in Appendix A, Section A.2. The SCALE 4.4a CSAS25 method was used for all calculations of this appendix.

E.3 SCALE 4.4a NCS Models

An arbitrary storage vault model was selected. The vault model had an interior size of 609.6 cm by 609.6 cm by 304.8 cm tall (20-ft by 20-ft by 10-ft tall) with a 60-cm thick concrete reflector on all six sides. Magnuson's Concrete (MGCONCRETE, from the SCALE 4.4a premixed material library) was used for the concrete model. A 7 x 7 x 2 array of DOT 9975 containers (same container and payload model of case c01 of Appendix C) was modeled in a corner of the vault.

A 6 x 6 x 3 array of HEU metal spheres was included in the vault model. One side of the HEU array was adjacent to the edge of the DOT 9975 array; another side of the HEU array was adjacent to a concrete wall. The array has an arbitrary "normal" condition as the initial array configuration, in that the modeled center-to-center spacing of the HEU items is 50.8 cm (20-inches).

The HEU metal spheres were modeled as being 100% ^{235}U at a density of 18.74 g/cm³ (input atom density of $N_{235} = 4.8014 \times 10^{-2}$ a/bn-cm). The modeled sphere radius was 6.3395 cm (5-inch diameter).

An isometric, sectional view of the storage model for normal conditions is shown by Fig. E.1 below. In Fig. E.1, the view cuts through the origins of the lowest level of the HEU units (upper units not shown), and the $^{237}\text{NpO}_2$ spheres may be seen in the cut through view of the DOT 9975 containers. Figure E.2 shows a cross-sectional graphic of the same configuration.

For the near-critical $6 \times 6 \times 3$ HEU array, the center spacing of the spheres was modeled as 33.02 cm (13-inches). Two more near-critical HEU arrays were modeled: a $3 \times 3 \times 3$ HEU array with 24.13 cm center spacing (9.5-inches) and a $2 \times 2 \times 2$ array with 17.145 cm center spacing (6.75-inches). As the size of the HEU array was decreased, the HEU array position was maintained adjacent to the DOT 9975 array and one concrete wall.

In cases where the DOT 9975 container array is omitted, the HEU array is placed in the corner previously occupied by the DOT 9975 array. This results in the HEU array having "corner" reflection by concrete.

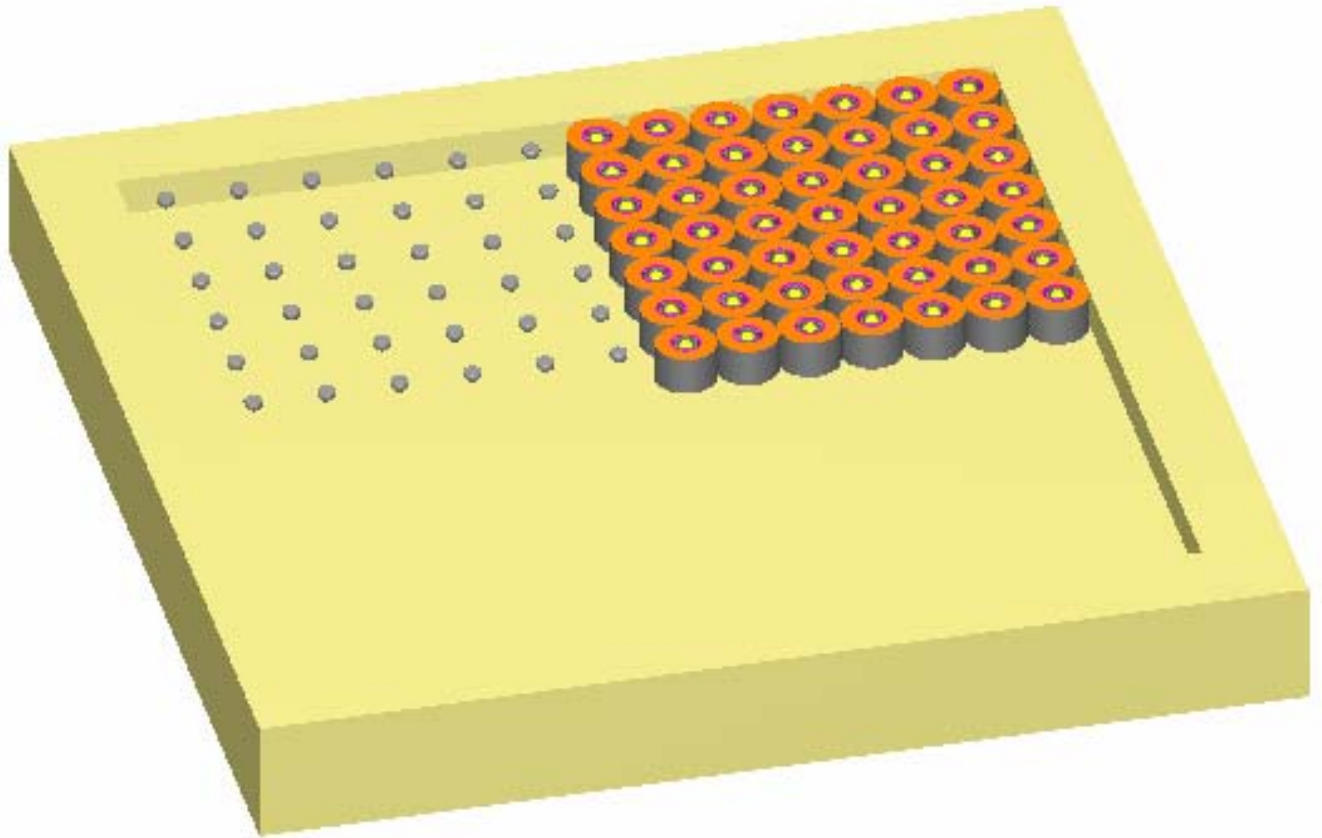


Fig. E.1 Graphic 1 of Mixed- Array Normal Condition Model

The 7×7 array of $^{237}\text{NpO}_2$ payloads may be seen in the cut-through view of the DOT 9975 containers. Items not shown in the graphic include the vault walls, ceiling, upper two layers of the $6 \times 6 \times 3$ HEU array, and the top layer of the $7 \times 7 \times 2$ DOT 9975 array. 50.8 cm center spacing of HEU units is shown.

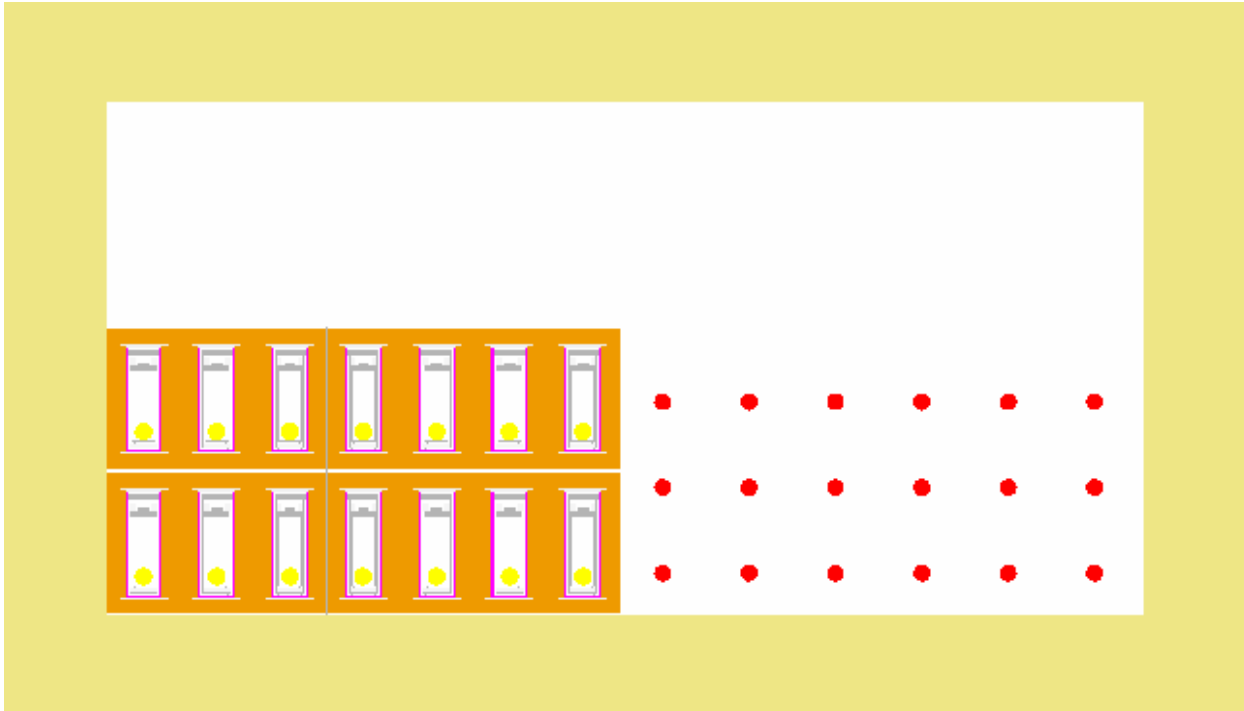


Fig. E.2 Graphic 2 of Mixed- Array Normal Condition Model
Cross-section view of same array depicted in Fig. E.1.

All cases employed 510 generations of 1000 neutrons, with a minimum of the first 10 generations discarded. Thus, each Monte Carlo result was based on $\sim 500,000$ neutron histories. The Monte Carlo standard deviation (σ) for all cases was ~ 0.0012 .

Fig. E.3 provides a sample input.

Fig. E.3. Sample SCALE 4.4a Input

(Input file ms02 - Near-critical 6 x 6 x 3 HEU array next to 7 x 7 x 2-unit DOT 9975 container array)

```
=csas25      parm=size=1000000
case mixed storage 02 - 6x6x3 heu array at critical
238groupndf5 infhommedium
'material 1 - 237np02 @ 11.143 g/cc
np-237      1 0 2.4942e-02 end
o           1 0 4.9883e-02 end
'material 2 - celotex: c6h10o5 @ 0.20 g/cc
c           2 0 4.4569e-03 end
h           2 0 7.4282e-03 end
o           2 0 3.7141e-03 end
'material 3 - ss304 @ 7.9 g/cc
fe          3 0 6.0360e-02 end
mn          3 0 1.7321e-02 end
cr          3 0 1.6471e-02 end
si          3 0 1.6940e-03 end
c           3 0 3.1696e-04 end
ni          3 0 6.4834e-03 end
'material 4 - aluminum @ 2.7 g/cc
al          4 0 6.0262e-02 end
'material 5 - aluminum honeycomb @ 0.28 g/cc
al          5 0 6.2494e-03 end
'material 6 - mgconcrete @ 2.1472 g/cc
mgconcrete 6 1.0          end
'material 7 - lead @ 11.29 g/cc
pb          7 0 3.2813e-02 end
'material 8 235u at 18.74 g/cc
u-235      8 0 4.8014e-02 293 end
end comp
more data dab=2000 end
case mixed storage 02 - 6x6x3 heu array at critical
read param
gen=510 npg=1000 nsk=10 nub=yes nb8=2000 tba=5 tme=360
end param
read geom
unit 1
com='payload elevation of 9975'
com=' w/ 6 kg np as th dens npo2 sphere'
sphere     1 1 5.26442 origin 0.0 0.0 23.3775
cylinder   0 1 6.571 59.12 18.113
cylinder   3 1 7.144 59.12 17.539
cylinder   0 1 7.702 59.12 17.539
cylinder   3 1 8.414 59.12 17.539
cylinder   0 1 9.525 59.12 17.539
cylinder   7 1 10.795 59.12 17.539
cylinder   2 1 21.415 59.12 17.539
cylinder   3 1 21.536 59.12 17.539
cuboid     0 1 4p21.536 59.12 17.539
unit 2
com='top of primary containment - ss304 pcv lid'
cylinder   3 1 7.455 62.61 59.12
cylinder   0 1 7.702 62.61 59.12
cylinder   3 1 8.414 62.61 59.12
cylinder   0 1 9.525 62.61 59.12
cylinder   7 1 10.795 62.61 59.12
cylinder   2 1 21.415 62.61 59.12
cylinder   3 1 21.536 62.61 59.12
cuboid     0 1 4p21.536 62.61 59.12
unit 3
com='primary containment ss304 nut and al honeycomb'
cylinder   3 1 3.175 63.90 62.61
cylinder   0 1 4.763 67.06 62.61
cylinder   5 1 7.702 67.06 62.61
cylinder   0 1 7.702 68.49 62.61
cylinder   3 1 8.414 68.49 62.61
cylinder   0 1 9.525 68.49 62.61
cylinder   7 1 10.795 68.49 62.61
cylinder   2 1 21.415 68.49 62.61
cylinder   3 1 21.536 68.49 62.61
cuboid     0 1 4p21.536 68.49 62.61
```

Fig. E.3. Sample SCALE 4.4a Input (Continued)

```
unit 4
com='top of secondary containment - ss304 scv lid'
cylinder 3 1 9.042 71.98 68.49
cylinder 0 1 9.525 71.98 68.49
cylinder 7 1 10.795 71.98 68.49
cylinder 2 1 21.415 71.98 68.49
cylinder 3 1 21.536 71.98 68.49
cuboid 0 1 4p21.536 71.98 68.49
unit 5
com='al shield top'
cylinder 0 1 9.525 73.27 71.98
cylinder 7 1 10.795 73.27 71.98
cylinder 4 1 10.795 74.54 71.98
cylinder 2 1 21.415 74.54 71.98
cylinder 3 1 21.536 74.54 71.98
cuboid 0 1 4p21.536 74.54 71.98
unit 6
com='pcv legs, al honeycomb and scv bottom'
cylinder 0 1 5.113 17.539 16.575
cylinder 3 1 5.715 17.539 16.575
cylinder 0 1 7.702 17.539 16.575
cylinder 5 1 7.702 17.539 14.034
cylinder 3 1 8.414 17.539 13.412
cylinder 0 1 9.525 17.539 13.412
cylinder 7 1 10.795 17.539 13.412
cylinder 2 1 21.415 17.539 13.412
cylinder 3 1 21.536 17.539 13.412
cuboid 0 1 4p21.536 17.539 13.412
unit 7
com='scv legs and bottom of lead shield'
cylinder 0 1 6.410 13.412 12.447
cylinder 3 1 7.065 13.412 12.447
cylinder 0 1 9.525 13.412 12.447
cylinder 7 1 10.795 13.412 11.177
cylinder 2 1 21.415 13.412 11.177
cylinder 3 1 21.536 13.412 11.177
cuboid 0 1 4p21.536 13.412 11.177
unit 8
com='al top plate and celotex plus void plus drum'
cylinder 4 1 14.224 75.81 74.54
cylinder 2 1 21.415 84.70 74.54
cylinder 0 1 21.415 85.847 74.54
cylinder 3 1 21.536 85.968 74.54
cuboid 0 1 4p21.536 85.968 74.54
unit 9
com='al bottom plate and celotex plus void plus drum'
cylinder 4 1 14.224 11.177 9.907
cylinder 2 1 21.415 11.177 1.271
cylinder 0 1 21.415 11.177 0.121
cylinder 3 1 21.536 11.177 0.000
cuboid 0 1 4p21.536 11.177 0.000
unit 10
array 1 -21.536 -21.536 0.0
unit 11
com='7x7x2 9975 array'
array 2 3*0.0
cuboid 0 1 301.504 0.0 609.6 0.0 304.8 0.0
replicate 6 1 0.0 5r60.0 1
unit 12
com='235u metal sphere in void cuboid'
sphere 8 1 6.3395
cuboid 0 1 6p16.51
unit 13
com='6x6x3 235u metal sphere array'
array 3 3*0.0
cuboid 0 1 308.096 0.0 609.6 0.0 304.8 0.0
replicate 6 1 60.0 0.0 4r60.0 1
```

Fig. E.3. Sample SCALE 4.4a Input (Continued)

```
global
unit 14
array 4 -60.0 -60.0 -60.0
end geom
read array
ara=1 nux=1 nuy=1 nuz=9 fill 9 7 6 1 2 3 4 5 8 end fill
ara=2 nux=7 nuy=7 nuz=2 fill 98r10 end fill
ara=3 nux=6 nuy=6 nuz=3 fill 108r12 end fill
ara=4 nux=2 nuy=1 nuz=1 fill 11 13 end fill
end array
read mixt
sct=3 eps=0.1
end mixt
end data
end
```

E.4 Results and Conclusions

Table E.1 provides the results of SCALE 4.4a calculations (CSAS25 routine) for the mixed-array configurations.

The computational results support that:

- (1) There appears to be no meaningful neutron interaction between $^{237}\text{NpO}_2$ -loaded DOT 9975 containers and adjacent near-critical arrangements of unmoderated HEU metal units. This implies that for less-reactive normal conditions of HEU storage, negligible neutron interaction exists.
- (2) The primary effect of presence of a DOT 9975 container array upon an immediately adjacent near-critical HEU arrangement is primarily that of a weak neutron reflector, due to the materials of construction of the DOT 9975 container. For the HEU storage, a concrete wall is a more effective reflector than an array of $^{237}\text{NpO}_2$ -loaded DOT 9975 containers.

The potential for criticality of HEU materials may be judged independent of the presence of $^{237}\text{NpO}_2$ -loaded DOT 9975 storage containers. The effect of the DOT 9975 container presence is no different than that afforded by structural presence of typical DOT Type B containers that may be commonly employed as HEU storage containers.

**Table E.1. SCALE 4.4a Results:
Adjacent Arrays of DOT 9975 Containers and HEU Units**

Case Name	HEU Unit Spacing (cm)	Configuration	k_{eff}	σ	EALF (MeV)
ms01	50.80	"Normal" condition for HEU array (6 x 6 x 3 array of 108 units)	0.9123	0.0011	0.225
ms02	33.02	Near-critical array involving very large number of HEU units (6 x 6 x 3 array of 108 units)	1.0085	0.0013	0.237
ms03	33.02	Like ms02, void $^{237}\text{NpO}_2$ material. (Empty DOT 9975 containers remain)	1.0117	0.0011	0.235
ms04	33.02	Like ms02, void ^{235}U material (Simulates absence of the HEU array).	0.4206	0.0007	1.645
ms05	33.02	Like ms02, no DOT 9975 array, HEU array is in corner.	1.0263	0.0011	0.224
ms06	24.13	Near-critical array involving large number of HEU units (3 x 3 x 3 array of 27 units)	0.9986	0.0012	0.371
ms07	24.13	Like ms06, void $^{237}\text{NpO}_2$ material. (Empty DOT 9975 containers remain)	0.9963	0.0012	0.375
ms09	24.13	Like ms06, no DOT 9975 array, HEU array is in corner.	1.0238	0.0012	0.333
ms10	17.145	Near-critical array involving a few HEU units (2 x 2 x 2 array of 8 units)	1.0013	0.0011	0.457
ms11	17.145	Like ms10, void $^{237}\text{NpO}_2$ material. (Empty DOT 9975 containers remain)	0.9998	0.0012	0.457
ms13	17.145	Like ms10, no DOT 9975 array, HEU array is in corner.	1.0327	0.0015	0.393

INTERNAL DISTRIBUTION

1. R. H. Elwood, Jr.
2. L. L. Gilpin
3. S. Goluoglu
4. M. A. Green
5. J. N. Herndon
6. D. J. Hill
7. C. M. Hopper
8. A. S. Icenhour
9. D. E. Mueller
10. C. V. Parks
- 11-15. D. A. Reed
16. C. M. Simmons
17. R. G. Taylor
18. R. M. Westfall
- 19-23. R. M. Wham
24. OTIC-RC, OSTI, CRL

EXTERNAL DISTRIBUTION

25. W. R. Brock, BWXT - Y-12, L. L. C., P. O. Box 2009, Oak Ridge, TN 37831
26. L. W. Boyd, DOE-ORO, Department of Energy, P. O. Box 2008 MS-6269, Oak Ridge, TN 37831
27. W. P. Carroll, DOE-HQ, NE-40/Germantown Building, U. S. Department of Energy, 1000 Independence Ave., S. W., Washington, D. C. 20585-1290.
28. S. O. Cox, BWXT - Y-12, L. L. C., P. O. Box 2009, Oak Ridge, TN 37831
29. R. A. Just, BWXT - Y-12, L. L. C., P. O. Box 2009, Oak Ridge, TN 37831
30. H. J. Keener, BWXT - Y-12, L. L. C., P. O. Box 2009, Oak Ridge, TN 37831
31. E. Kendall, NNSA, Department of Energy, P. O. Box 2001 MS-8193, Oak Ridge, TN 37831
32. R. C. McBroom, DOE-ORO, Department of Energy, P. O. Box 2001, Oak Ridge, TN 37831
33. S. R. Martin, Jr., DOE-ORO, Department of Energy, P. O. Box 2008 MS-6269, Oak Ridge, TN 37831
34. T. R. Miller, BWXT - Y-12, L. L. C., P. O. Box 2009, Oak Ridge, TN 37831
35. M. J. Plaster, BWXT - Y-12, L. L. C., P. O. Box 2009, Oak Ridge, TN 37831
36. K. H. Reynolds, DOE-ORO, Department of Energy, P. O. Box 2001, Oak Ridge, TN 37831

ELECTRONIC NOTIFICATION

37. C. H. Scott, ORNL (scottch@ornl.gov)
38. C. S. Sims, ORNL (simscs@ornl.gov)